Volume 72C
Number 3
July–Sept. 1968

Engineering and Instrumentation

U.S. DEPARTMENT OF COMMERCE

SECTION C

JOURNAL OF RESEARCH

NATIONAL BUREAU OF STANDARDS

Journal of Research
of the
National Bureau of Standards

C. Engineering and Instrumentation

July–Sept. • 1968

VOLUME • 72C

NUMBER • 3

Editor: Martin Greenspan

Associate Editors: G. F. Montgomery, R. V. Smith, A. F. Schmidt

Publication dates:
Feb. 15, May 15, Aug. 15, Nov. 15, 1968

JOURNAL OF RESEARCH

The National Bureau of Standards Journal of Research reports research and development in the fields of activity shown at right. Also included from time to time are survey articles on topics closely related to the Bureau's scientific and technical program.

The Journal is published in three separate sections as follows:

A. Physics and Chemistry

Contains papers of interest primarily to scientists working in these fields. Issued six times a year. Annual subscription: domestic, $5.00; foreign, $6.00. Single copy, $1.00.

B. Mathematical Sciences

Presents studies and compilations designed mainly for the mathematician and the theoretical physicist. Issued quarterly. Annual subscription: domestic, $2.25; foreign, $2.75. Single copy, 75¢.

C. Engineering and Instrumentation

Reports research and development results of interest chiefly to the engineer and the applied scientist. Issued quarterly. Annual subscription: domestic, $2.75; foreign, $3.50. Single copy, 75¢.

The National Bureau of Standards[1] was established by an act of Congress March 3, 1901. Today, in addition to serving as the Nation's central measurement laboratory, the Bureau is a principal focal point in the Federal Government for assuring maximum application of the physical and engineering sciences to the advancement of technology in industry and commerce. To this end the Bureau conducts research and provides central national services in three broad program areas and provides central national services in a fourth. These are: (1) basic measurements and standards, (2) materials measurements and standards, (3) technological measurements and standards, and (4) transfer of technology. The Bureau comprises the Institute for Basic Standards, the Institute for Materials Research, the Institute for Applied Technology, and the Center for Radiation Research.

THE INSTITUTE FOR BASIC STANDARDS provides the central basis within the United States of a complete and consistent system of physical measurement, coordinates that system with the measurement systems of other nations, and furnishes essential services leading to accurate and uniform physical measurements throughout the Nation's scientific community, industry, and commerce. The Institute consists of an Office of Standard Reference Data and a group of divisions organized by the following areas of science and engineering:

Applied Mathematics—Electricity—Metrology—Mechanics—Heat—Atomic Physics—Cryogenics[2]—Radio Physics[2]—Radio Engineering[2]—Astrophysics[2]—Time and Frequency.[3]

THE INSTITUTE FOR MATERIALS RESEARCH conducts materials research leading to methods, standards of measurement, and data needed by industry, commerce, educational institutions, and government. The Institute also provides advisory and research services to other government agencies. The Institute consists of an Office of Standard Reference Materials and a group of divisions organized by the following areas of materials research:

Analytical Chemistry—Polymers—Metallurgy—Inorganic Materials—Physical Chemistry.

THE INSTITUTE FOR APPLIED TECHNOLOGY provides for the creation of appropriate opportunities for the use and application of technology within the Federal Government and within the civilian sector of American industry. The primary functions of the Institute may be broadly classified as programs relating to technological measurements and standards and techniques for the transfer of technology. The Institute consists of a Clearinghouse for Scientific and Technical Information,[3] a Center for Computer Sciences and Technology, and a group of technical divisions and offices organized by the following fields of technology:

Building Research—Electronic Instrumentation—Technical Analysis—Product Evaluation—Invention and Innovation—Weights and Measures—Engineering Standards—Vehicle Systems Research.

THE CENTER FOR RADIATION RESEARCH engages in research, measurement, and application of radiation to the solution of Bureau mission problems and the problems of other agencies and institutions. The Center for Radiation Research consists of the following divisions:

Reactor Radiation—Linac Radiation—Applied Radiation—Nuclear Radiation.

[1] Headquarters and Laboratories at Gaithersburg, Maryland, unless otherwise noted; mailing address Washington, D.C. 20234.
[2] Located at Boulder, Colorado 80302.
[3] Located at 5285 Port Royal Road, Springfield, Virginia 22151.

U.S. DEPARTMENT OF COMMERCE
C. R. Smith, Secretary
NATIONAL BUREAU OF STANDARDS
A. V. Astin, Director

Order all publications from the Superintendent of Documents
U.S. Government Printing Office, Washington, D.C. 20402.

Use of funds for printing this publication approved by the Director of the Bureau of the Budget (June 22, 1966).

JOURNAL OF RESEARCH of the National Bureau of Standards—C. Engineering and Instrumentation
Vol. 72C, No. 3, July–September 1968

Gas Density Balance Design Considerations

E. C. Creitz

Institute for Applied Technology, National Bureau of Standards, Washington, D.C. 20234

(May 2, 1968)

The Nerheim gas density balance operates by measuring the flow produced by differences in density between a sample and a reference gas in the earth's gravitational field. It has been considered theoretically in order to outline the characteristics of the gas flow system, those of the flow measuring anemometers, and the effects of detector volume on peak separation and sensitivity. It is shown that both design parameters and operating conditions affect the performance of the device, and that properly considered compromises can improve its characteristics.

Key Words: Chromatographic detector; density detector; gas density; gas detector.

1. Introduction

The Nerheim version [1][1] of the Martin gas density balance [2, 3] presents a number of advantages over other detectors for gas chromatography, not the least of which are its ease of calibration, and its adaptability to the measurement of corrosive column effluents. Ease of calibration is attributable to the "absolute" [4] nature of its output, being directly related to density difference between reference gas and column effluent. Corrosion resistance is achieved by handling the corrosive gases in ducts of resistant material so that the sample is not lost, while maintaining the sensing elements in an inert atmosphere, so that they, also, are not destroyed.

Nerheim [1] presented an analysis of the energy balance in the pneumatic parts of the detector. However, the information given was not of a type readily adaptable to instrument design. The study presented here was undertaken in an attempt to separate design parameters of a fixed nature from those which may be varied, and to define more clearly the variables affecting the overall response of the system to changes in density of the column effluent.

2. Pneumatic System

A schematic representation of the Nerheim gas density balance is shown in figure 1, the lines representing ducts through which gases flow. The principle of operation is remarkably simple. Since its operation depends on gravitational effects, the duct system of figure 1 is arranged so that duct BD, and those shown parallel to it, must be vertical. Reference gas enters at A and the flow splits so that, theoretically, equal amounts pass over the flow detectors, F. Column effluent enters at C, and also splits so that equal amounts flow to B and D, where the column effluent and reference gas mix and finally exit at G. Thus, with the reference gas supplied to both the column and the detector, and no eluted compounds in the column effluent, a state of dynamic flow balance exists. Eluted compounds in the column effluent disturb the dynamic balance by causing an additional flow, ΔQ, downward (if the eluate is more dense than the reference gas) in the center leg B–D. The disturbance in the dynamic equilibrium is transmitted into arms 1 and 2, where its magnitude is measured by the transducers F. One may note two fixed design characteristics at this point.

(1) Symmetry in the gas flows above and below the horizontal line ACG implies the requirement of symmetry in the duct dimensions about the same line.

(2) The driving force producing the disturbance in the flow rates is directly proportional [1] to the vertical height of the center section B–D of figure 1.

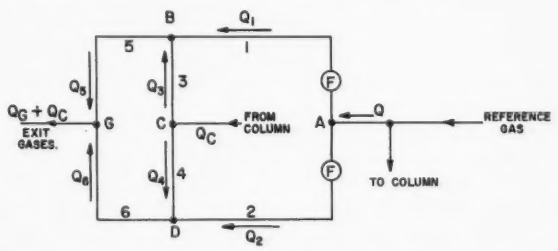

FIGURE 1. *Diagrammatic representation of the Nerheim gas density balance showing location of detector units F, and directions of gas flow.*

The lines represent ducts through which gases flow.

[1] Figures in brackets indicate the literature references at the end of this paper.

Gravitational effects appear in the vertical sections of both branches 3–4 and 5–6 and cause changes in flow in each of the branches. However, if the flow transducers are to be kept out of contact with the column eluate in order to protect both the transducers and the sample, a third condition is imposed.

(3) Flow measuring elements are to be installed in branches 1 and 2. This condition has certain implications with respect to reflection of flow disturbances into the ducts containing the transducers. It implies that, to be effective in protecting both transducers and sample, an operational factor must be controlled, namely, the flow in branches 1 and 2 should be high enough to prevent back diffusion of sample into these branches. As will be seen later, this condition results in a compromise in the selection of an appropriate flow rate.

At low Reynolds numbers (in this case 50), viscous flow occurs and Poiseuille's expression for the flow of a fluid through a conduit of circular cross section permits the construction of an electrical analog for the gas flows in the pneumatic system. To a first approximation the volume, Q, of gas flowing per unit time through a conduit of radius, r, and length, L, is given by

$$Q=\frac{\pi P r^4}{8\eta L} \tag{1}$$

in which P is the pressure-difference between the ends of the conduit and η is the viscosity of the gas flowing through it. In the electrical analog the electrical current, I, corresponds to the "pneumatic current", Q; the electrical voltage drop, E, across a resistance corresponds to the pressure drop, P, between the ends of the conduit; and the electrical resistance, R, to the frictional resistance $\frac{8\eta L}{\pi r^4}$ in the pneumatic system. The electrical analog for the pneumatic system in dynamic balance is shown in figure 2. The current measuring devices shown as F_1 and F_2 are presumed to be (in the case of the analog) the sensing elements of a differential ammeter. Condition 1, requiring symmetry about the horizontal center-line stipulates that, for the electrical analog $R_1=R_2$, $R_3=R_4$ and $R_5=R_6$. Figure 2 represents the balanced pneumatic system in the absence of a sample in the column effluent, so that $I_1=I_2$, $I_3=I_4$ and $I_5=I_6$. The presence of an eluate, having a density greater than the carrier gas, causes a reduction in Q_3 and an increase in Q_4 (rates of flow in arms 3 and 4) of figure 1, which corresponds to a decrease in I_3 and an increase in I_4 of figure 2. The total current in each part of the system may, therefore, be considered to be the sum of two currents—the one corresponding to the dynamic equilibrium in the absence of sample in the column effluent, and the other an internally circulating current due to the presence of such a sample. The differential flow detector is designed specifically to balance out the signals related to the flows associated with the dynamic equilibrium and to measure only the flow associated with the internal current caused by the difference in density of the sample. The electrical analog corresponding to the internal flow is shown in figure 3a, and with lumped curcuit elements in figure 3b. The battery, E, in the figures, represents the pressure, ΔDgh, causing the internal flow (ΔD = density difference between the contents of arms A and C of figure 1, g = the local acceleration of gravity, and h = the vertical height of the gas column in the central arm, C, of fig. 1). The density difference also appears in the exit branch (G of fig. 1) but its effect on the flows in the other branches will be neglected until after discussion of the circuit of figure 3b. For this circuit one may write

$$I_C=I_A+I_G \tag{2}$$

and

$$E=I_C R_C+I_A R_A=I_C R_C+I_G R_G \tag{3}$$

from which one obtains the expression

$$E=I_A\left(R_A+R_C+\frac{R_A R_C}{R_G}\right) \tag{4}$$

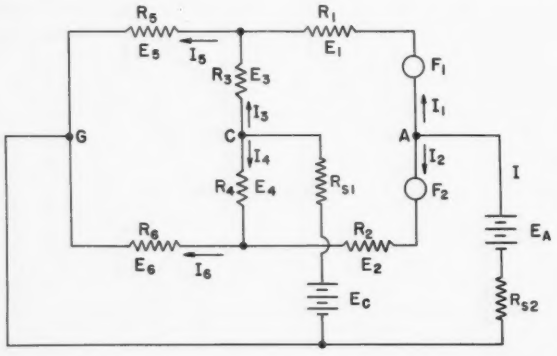

FIGURE 2. *Electrical analog for the pneumatic circuit of figure 1 showing current paths for the case when no sample is present in the column effluent, representing only reference gas flow through the balance.*

R_{s2} is the source resistance for E_A. It consists of the regulator and needle valves. R_{s1} is the source resistance for E_C, consisting of an additional needle valve and the resistance of the column. Both R_{s1} and R_{s2} are high compared to the other resistances in the system.

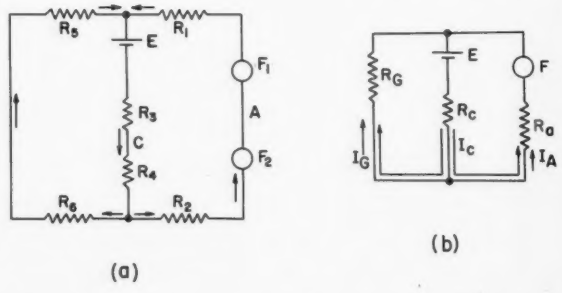

FIGURE 3. (a) *Electrical analog of the pneumatic system of figure 1 showing only currents related to the presence of sample in the column effluent. (Internal gas flow).* (b). *The same as 3a except that the circuit constants are lumped.*

$R_c=R_3+R_4$ is the source resistance for E. It contains such factors as L_3+L_4, η, r_3^4 and r_4^4.

Current flowing in the G branch is not measured by the detector, F, and thus, constitutes a loss in sensitivity. In order for the detector, F, to measure a large fraction of the current, I_C, the resistance, R_G, must be large. If $R_C + R_A \gg \frac{R_A R_C}{R_G}$ the last term in eq (4) may be neglected, and $I_A = I_C = I$. The sensitivity, in terms of units of flow per unit of pressure becomes

$$\frac{I}{E} = \frac{1}{R_C + R_A} = \frac{1}{4R} \tag{5}$$

in the electrical analog. The above considerations lead to the design condition:

(4) The pneumatic resistance in the G branch should be high compared to that in the A and C arms of figure 1. Considering symmetry requirements along with condition 4, leads to

$$\frac{L_5}{r_5^4} + \frac{L_6}{r_6^4} \gg \frac{L_1}{r_1^4} + \frac{L_2}{r_2^4} + \frac{L_3}{r_3^4} + \frac{L_4}{r_4^4}$$

$$\text{and } \frac{L_5}{r_5} = \frac{L_6}{r_6}, \frac{L_1}{r_1} = \frac{L_2}{r_2}, \frac{L_3}{r_3} = \frac{L_4}{r_4}.$$

For that part of the circuit involving only the A and C branches of figure 3a, the total resistance around the circuit is $R_1 + R_2 + R_3 + R_4$. The pneumatic equivalent of the Ohms law equation becomes:

$$\Delta Q = \frac{\Delta D g h}{\frac{8\eta'}{\pi}\left(\frac{L_1}{r_1^4} + \frac{L_2}{r_2^4} + \frac{L_3}{r_3^4} + \frac{L_4}{r_4^4}\right)}.$$

If $L_1 + L_2 + L_3 + L_4 = L$ and $r_1 = r_2 = r_3 = r_4 = r$

$$\Delta Q = \frac{\pi g h r^4}{8\eta L} \Delta D. \tag{6}$$

For convenience, the assumptions used in the derivation of eq (6) are summarized and discussed below.

1. It was assumed that the A- and C-branches had the same (low) resistance to flow and that the G-branch had high resistance to flow. Since most potentiometric recorders cannot resolve signals much smaller than about 0.5 percent there is little point in making the total resistance in the G-branch more than 200 times that in the A- and C-branches. Note that, in the derivation of eq (6), it cannot be assumed that $R_g = \infty$ because this assumption would lead to a system with two inlets and no outlet, and the balance could not work. However, a moderate increase in the overall pressure drop could increase the sensitivity by way of an increase in ΔD.

2. The assumption of laminar flow in the A- and C-branches appears to be justifiable for Reynolds numbers of about 50 and below.

3. The viscosity of the carrier gas was considered to be identical to that of the reference gas. For the case of ducts of uniform radius, the resistance to flow around the A- and C-branch loop is proportional to $\eta_1\left(\frac{L}{2r^4}\right) + \eta_2\left(\frac{L}{2r^4}\right) = \frac{\eta_1 + \eta_2}{2}\left(\frac{L}{r^4}\right)$. Depending somewhat on the column and the nature of the sample gas, the actual concentration of sample in the carrier gas is of the order of 0.5 percent. If it is assumed that the viscosity change on mixing is proportional to the amount of sample in the carrier gas, the change in resistance to flow would have a maximum value of 0.5 percent of the average of their viscosities. Additionally, the small error from this source would become smaller with an increase in detector sensitivity which would permit the use of a smaller sample.

4. The effects of gravitationally induced flow in the G-branch on the internal flow measured in the A-branch would be small for two reasons. Such a flow must overcome a resistance which is large compared to that in the A- and C-branches taken as a parallel circuit and secondly, the force producing the flow in the G-branch is less than that in the C-branch by a factor of $\frac{Q_c}{Q_c + Q}$ because of dilution at points B and D of figure 1. For example, if $R_G = 100\ (R_C + R_A)$ and for $Q_C = 25$ and and $Q = 150$ cm^3 min^{-1} the amount of flow reflected into the A- and C-branches would be only 0.14 percent of the internal flow produced by $\Delta D g h$ in the C-branch.

5. The flow measuring devices (F in fig. 1) were assumed to introduce no resistance to flow in the A-branch. The error introduced by this assumption depends on the skill of the designer, but presumably it can be made small at the low velocities expected.

6. The effects of T-joints and 90° bends on the resistance to flow in the A- and C-branches were assumed to be negligible. Such resistances depend primarily on the velocity of gas flow, and at constant flow rate, they are also constant. Some estimates of the magnitude of such resistances in relation to the resistance of the straight sections of the ducting are made in the appendix, q.v. For a balance having ducting of 1/4 in diam with a reference gas N_2 flow rate of 150 cm^3 min^{-1}, and a carrier gas flow rate of 25 cm^3 min^{-1}, a height of 45 to 60 cm would be required to reduce the error caused by the neglect of resistances in T-joints and bends to 1 percent of that in the straight sections, the required height being a function of the ratio of the radius of curvature of the elbows to their pipe radius.

In accordance with the notation of figure 1, let Q_0 be the flow in each of the branches 1 and 2 when no sample is present in the central branch. When sample is present $Q_1 = Q_0 + \Delta Q$ and $Q_2 = Q_0 - \Delta Q$ in which ΔQ is the volume rate of internal flow associated with the density difference ΔD. The detectors are sensitive to velocity rather than to volumetric flow rate. Thus, for ducts of equal diameter one may write:

$$\frac{Q_1 - Q_2}{Q_0} = \frac{2\Delta Q}{Q_0} = \left(\frac{\pi g h r^4}{8\eta L Q_0} \Delta D\right) \times 2$$

Since velocity is directly related to volumetric flow rate

$$\frac{v_1 - v_2}{v_0} = \frac{2\Delta_v}{v_0} = \frac{\pi g h r^4}{2\eta L Q} \Delta D \tag{7}$$

in which $Q = 2Q_0$ is the total amount of reference gas flowing per second into the system at point A, figure 1, Δv is the velocity of internal flow and v_0 is the velocity in branches 1 or 2 when no sample is present. Equation 7 indicates that, subject to the foregoing design limitations and at constant operating conditions, the relative change in velocity is linear with respect to the density difference between the contents of branches A and C.

Equation (7) contains no references to values applicable to the exit branch, G, it being required only that the resistance in this branch be sufficiently large. The requirement for high resistance is reduced somewhat when the effect of gravitation in the exit branch is considered. Figure 4 is a modification of figure 3b to show the effect of gravitational pressure in the exit branch. E_G is polarized in such a direction as to oppose the flow of internal current in the G-branch and adds to the voltage drop across R_G produced by the internal current.

3. Measurement of Gas Velocities

Hot wire anemometers are conventionally used as transducers for the conversion of gas velocities into electrical signals. One of the requirements imposed on the transducer is that it liberate little heat energy into the gas stream. Such heat release can result in stack action (chimney effect) producing an internal flow independent of the density difference which is to be measured. On the other hand, the transfer of heat energy to the gas stream from the hot anemometer element is the principle on which conventional anemometers operate. Obviously a compromise is in order, and a limit is set on the ultimate sensitivity attainable, which depends, somewhat, on the location of the anemometers in the pneumatic system. While thermistor elements have higher temperature coefficients of resistance and may liberate somewhat less heat for a comparable sensitivity than do wire elements, they are subject to drift and are hard to obtain in pairs sufficiently well matched both thermally and electrically.

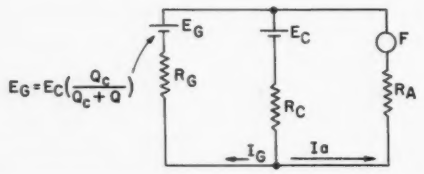

FIGURE 4. *Electrical analogue circuit of figure 3b with potential source added to represent gravitational forces in the exit branch.*

(Internal gas flow only) R_g is the source resistance of E_G. It includes such factors as $L_3 + L_a$, η, r_3^4 and r_a^4.

Their use has been covered elsewhere [1]. Wire elements must be made from small enough wire (in the order of 0.0001 in) to be sufficiently sensitive and liberate negligible amounts of heat energy. Their disadvantage is that they are fragile. When properly aged they are subject to much less drift than thermistors, and their time constants are negligible compared to that of the usual strip-chart recorder. In general, the properties of hot wire anemometers appear to be adequate for the intended use, particularly if the design variables of both the electrical and pneumatic systems are optimized.

Hot wire anemometers may be used either as constant resistance or as constant current devices [5]. Operation as constant resistance devices implies certain difficulties in that a single anemometer must be used and the voltage to the Wheatstone's bridge or the current through it must be varied in such a way as to maintain bridge balance. Conversely, operation of a pair of anemometers as constant current devices presents few problems and has the added advantage that a properly connected bridge can be self-compensating with respect to current changes caused by resistive changes in the sensing elements. Since the resistive change in one anemometer is equal and opposite to that in the other, the total bridge resistance remains constant, as does the voltage across the bridge. Such a bridge is shown in figure 5. It should be noted that the circuit of figure 5 is not a true Wheatstone's bridge in that the potentiometric recorder bucks out all voltage across the "galvanometer arm" of the bridge so that no current flows through it. The circuit should be regarded as a fixed and a variable voltage divider connected in parallel, the junction between resistors S_1 and S_2 acting as the fixed reference potential.

The velocity, v, of gas flow over a hot wire anemometer element is related to the resistance of the element at operating temperature, R, and its resistance at ambient temperature, R_a, by the equation

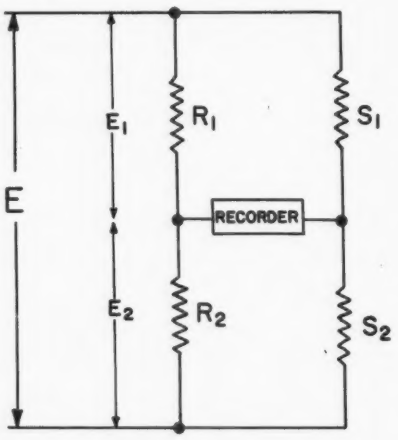

FIGURE 5. *The electrical measuring circuit showing the connections to the anemometers,* R_1 *and* R_2*, and to standard resistors* S_1 *and* S_2.

$$\frac{I^2R}{R-R_a}=M\sqrt{v}+B$$

in which I is the current supplied to the element. If I is made constant, it may be combined with M and B to give

$$\frac{R}{R-R_a}=m\sqrt{v}+b$$

The straight-line relationship of figure 6 applies only at velocities sufficiently high so that the effects of thermal convection are negligible. Below this particular velocity the slope falls off and approaches zero or even reverses in sign [5]. A typical curve, obtained by calibration in the instrument, is shown in figure 6.

Proper matching of a pair of anemometers implies another design criterion.

(5) Within "reasonable" limits, the values of m and b in eq (13) should be the same for each of a pair of matched wire anemometers.

If m_1 is assumed equal to m_2 and $b_1=b_2$ for such a matched pair, the fractional change in resistances must be equal, i.e., $\frac{R_1-Ra_1}{R_1}=\frac{R_2-Ra_2}{R_2}$, for the same velocity of gas flow across them. In order for them to show this characteristic it is impractical that they be physically very different so that it is reasonable to assume that $Ra_1=Ra_2=Ra$, and, for equal velocities of flow across the wires (no sample in the C-branch), $R_1=R_2=R$. For the off-balance condition, with internal flow present, $R_1=R-\Delta R$ and $R_2=R+\Delta R$, assuming the sample to be more dense than the carrier gas. The fractional change in the velocity caused by the internal flow produces resistive changes given by

$$\frac{v_1-v_2}{v_0}=\frac{2\Delta v}{v_0}$$

$$=\frac{\left[\frac{R-\Delta R}{R-\Delta R-Ra}-b\right]^2-\left[\frac{R+\Delta R}{R+\Delta R-Ra}-b\right]^2}{\left[\frac{R}{R-Ra}-b\right]^2} \qquad (14)$$

which simplifies to

$$\frac{\Delta v}{v_0}=2\Delta R\left[\frac{-Ra}{R(R-Ra)-b(R-Ra)^2}\right]=2K\Delta R \qquad (15)$$

in which

$$K=\frac{-Ra}{R(R-Ra)-b(R-Ra)^2}.$$

The negative sign is an indication that the slope of the $\frac{R}{R-R_a}$ versus $v^{\frac{1}{2}}$ line is opposite to that of the R versus $v^{\frac{1}{2}}$ line. The sign of K has no practical significance since it is easily taken care of by reversing the polarity of the batteries driving the bridge. Substituting from eq (7)

$$\Delta R=\frac{1}{K}\left(\frac{\pi gh}{8\eta L}\right)\frac{r^4}{Q}\Delta D \qquad (16)$$

The signal to the recorder, ΔE, is $I\Delta R$, considering the wires in series as a simple voltage divider, so that

$$\Delta E=\frac{\pi ghr^4I}{8\eta KLQ}\Delta D. \qquad (17)$$

If the current, I, is expressed in milliamperes, the overall sensitivity in units of millivolts per gram-cm^3 is

$$\frac{\Delta E}{\Delta D}=\frac{\pi ghr^4I}{8\eta KLQ}. \qquad (18)$$

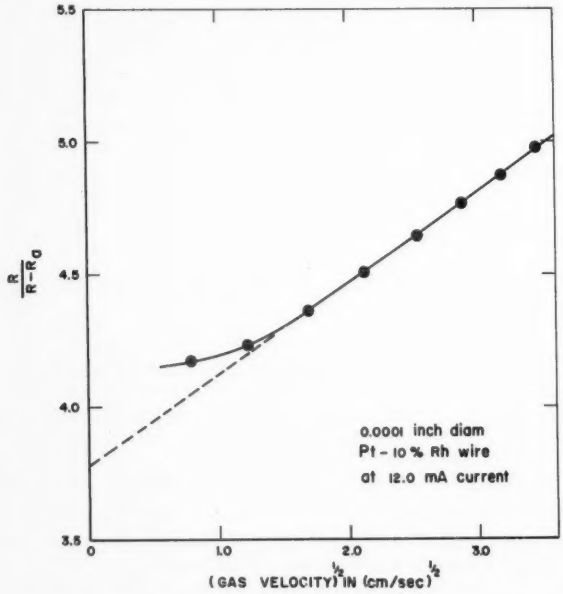

FIGURE 6. *Calibration curve for a hot wire anemometer, showing the effect of convection currents at low gas velocities.*

4. Detector Volume

The volume of sample plus carrier gas included in the detector is of major concern where either the size of the available sample is small or where minor constituents of a mixture are to be determined. The rather large dividends in detector sensitivity realized from rather small increases in its radius requires that some consideration be given to the effects of the increased detector volume on the shapes of recorded peaks. When the area under the peak is to be used as a measure of the amount of an eluted constituent, it is imperative that peaks do not overlap, if the area

measurements are to be made accurately. The separation of recorded peaks depends on both the detector and the column and, to a certain extent, the overlapping caused by a large detector volume can be compensated for by a redesign of the column. It seemed desirable, therefore, to estimate the increase in the sensitivity of the detector in terms of the increase in peak width resulting from an increase in detector volume, assuming the increase in volume to be obtained by way of an increased radius, the height remaining fixed. It should be noted that the volume of interest is that of the C-branch alone.

A qualitative understanding of the effects of detector volume in a real detector operating on a real sample can be had by comparison with a hypothetical detector working on a hypothetical sample. Assume a hypothetical sample of one arbitrary unit of volume, contained in a tube between two sections of carrier gas, from which it is discharged into a hypothetical detector, the volume of which may be changed at will without affecting its sensitivity. It will further be assumed that no mixing occurs so that the sample has planar leading and trailing edges and that it is introduced directly (no column) into the detector. It may be assumed, first, that the detector has infinitely small volume so that it is either completely filled or completely empty of sample at any given instant. The output of such a detector with such a sample would be a square wave. A detector having the same volume as the sample is more realistic. Its output would take the form of an isosceles triangle, the detector being completely filled at only one instant. Similarly, for detectors having volumes greater than the hypothetical sample, the output would have the shape of an isosceles trapezoid. In the above examples, three effects are to be noted. (1) When the detector volume exceeds one unit (equal the sample size) the maximum response decreases. (2) The width of the curve increases with increase in detector volume. (3) The area under the curve remains constant, because the detector measures all of the sample that passes through it to give a quantitative measure of the total amount of sample. For the case where some mixing can occur, the sharp corners of the curves would be rounded, the exit corners being somewhat more rounded than the inlet corners because of the increased time allowed for mixing.

Consider, next, the effect of the column on the same hypothetical sample. The effect is to retain the individual molecules for different times, depending on their individual energies, so that, at the column exit, the concentration would vary to approximate a normal distribution curve [6]. The hypothetical "ideal" detector, having zero volume, would follow the instantaneous concentration perfectly and give a recorded output which would also be a normal distribution curve. However, a nonideal detector, having a finite volume and responding to a constantly changing sample concentration, would give an instantaneous output corresponding to the average density of the contents of its C-branch. Its recorded peak would be a modified normal distribution curve, being somewhat wider and not as high at the maximum as that from the detector having zero volume. Thus, the larger the volume of the detector, the greater the area of the normal distribution curve which would be instantaneously averaged, and the lower and broader the recorded output would become.

The practical gas density balance more than compensates for the theoretical reduction in curve height, however, since its sensitivity increases as the square of its volume at constant detector height. The extent of the overcompensation is shown in figure 7 for some of the cases discussed above. Since a practical detector would have zero sensitivity at zero volume, no curves are shown for these cases. Curve A represents the output for a practical detector of one arbitrary unit of volume responding to a hypothetical sample of one unit of volume when the sample is introduced directly into the detector. The output would increase linearly until the detector was completely filled, then decrease linearly until it was completely empty. Curve B represents a similar situation except that the volume of the detector was taken as two arbitrary units. When the sample has been completely transferred to the detector, the sample represents only 50 percent of the total contents. However, the maximum output would be $0.5 \times (2)^2 = 2$. Curve C represents the output of a detector of three arbitrary units of volume when supplied with a sample of an arbitrary unit of volume. Similar reasoning was applied to the case where the sample was assumed to have passed through a column. For the output of the detector having zero volume, the coordinates were chosen such that the area under the curve was equal to one arbitrary unit. This curve was scanned by assumed detector volumes of 1, 2, 3, and 4 units and output values calculated. The curves were cut off at 99.9 percent of the full area under the curve and matched on the left to simulate the appearance of a sample at the detector inlet. They are shown as curves D, E, F, and G of figure 7. The areas under these four curves were plotted in figure 8 as a function of the width. Figure 8 indicates that an increase in detector volume of four units produced an increase in area of 1340 percent at a cost of about 30 percent in increased width.

5. Choice of Reference Gas

Equation 18 may be rewritten as $\Delta E \propto \frac{\Delta D}{\eta}$ assuming all the operational and design parameters to be constant and assuming the carrier gas to be the same as the reference gas. For a fixed volumetric concentration of sample in the carrier gas one may write $\Delta E \propto \frac{D_s - D_r}{\eta}$ in which D_r is the density of the reference gas and D_s is the density of the sample. If one further assumes that the sample has a density of 1 g/cm^3, one may calculate a relative response to be expected from several reference gases. This has been done and is shown in table 1. The gases in the list were chosen because

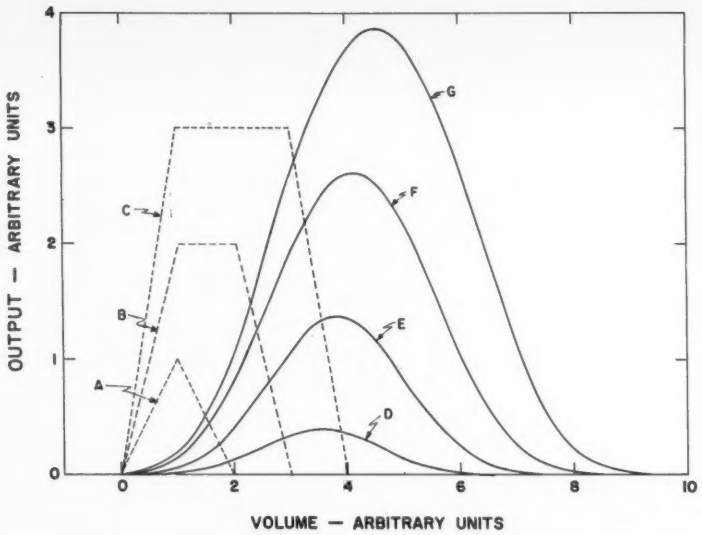

FIGURE 7. *The effect of increased detector output associated with increased detector volume at constant height.*

Curves A, B and C are for a hypothetical slug of sample having planar ends traversing detectors of volumes; A- equal to the sample volume; B- twice the sample volume, and C- three times the sample volume. Curves D, E, F, and G show the effect on detector output of the same 1-unit-of-volume sample after passing through a column, for detectors having volumes 1, 2, 3, and 4 times that of the sample.

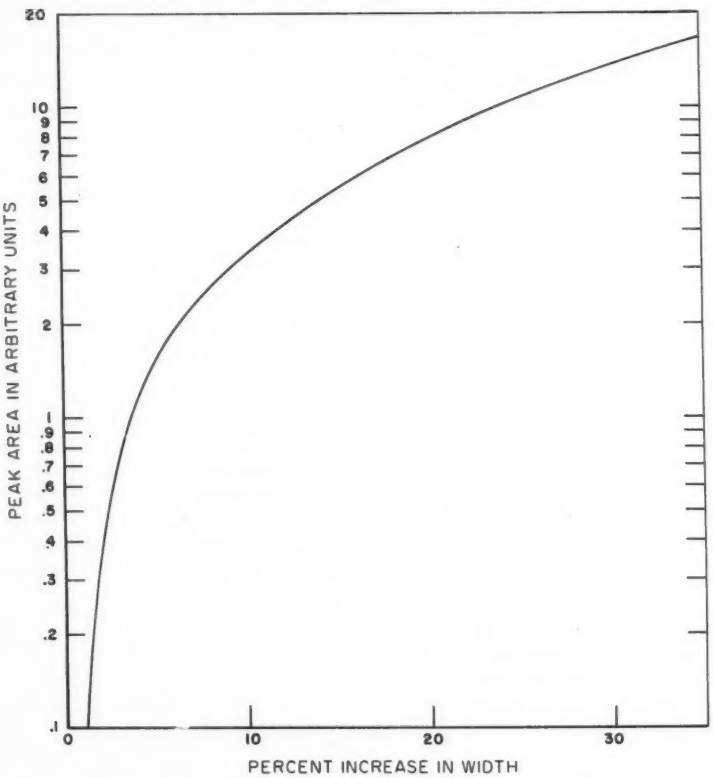

FIGURE 8. *The increase in peak area obtained at the expense of peak width when the detector volume is increased, the height remaining constant.*

TABLE 1

Gas	(gram cm^{-3} poise^{-1})
Hydrogen	10.4
Helium	4.1
Methane	3.1
Nitrogen	−0.6
Carbon monoxide	−0.8
Air	−1.0
Oxygen	−1.5
Ethylene	−1.5
Ethane	−2.6
Argon	−2.8
Carbon dioxide	−5.4
Propane	−10.0
Chloroethane	−15.3
n-Butane	−17.1
Bromomethane	−23.1
Chlorodifluoromethane	−24.6
Dichlorofluoromethane	−29.9
Sulfure hexafluoride	−30.2
Bromotrifluoromethane	−32.4
Dichlorodifluoromethane	−34.2
Trichlorofluoromethane	−45.4
Octafluorocyclobutane	−64.3

information on both density and viscosity were available. They were listed without regard to their toxic hazards or their suitability for use as chromatographic carrier gases. Such a table is useful in that the relative response for one of the gases as the sample in another as the reference gas may be obtained from the table.

Guilleman and Auricourt [7] made measurements of the effects of reference gases of different density on the performance of the gas density balance. They neglected the effects of flow rate, Q in eq (18), on sensitivity and the effects of using different carrier gases on resolution of the column. Accordingly, their results cannot be compared with those predicted from the table.

6. Discussion

An order of magnitude value for the probable sensitivity of the detector is of interest. Equation 18 may be rewritten as:

$$\frac{\Delta E}{\Delta D} = 2.18 \times 10^6 \left(\frac{h}{L}\right)\left(\frac{I}{K}\right)\left(\frac{r^4}{Q}\right) \text{millivolt per gram-cm}^{-3}$$

assuming room temperature and nitrogen as the reference gas. Values of the three quantities in parentheses will be estimated separately starting with the last one.

The results shown in figure 6 were obtained on an anemometer wire mounted horizontally in a 0.635 cm (1/4 in) I.D. hole in a brass block. The value of r was, therefore, fixed at 0.3175 cm and the smallest usable value of Q can be estimated from the curve of figure 6. However, the anemometers operate in opposite directions on the curve, and an operating point must be chosen which will allow each anemometer to operate in the linear region of its curve. For purposes of estimation we may choose to use the point at $\sqrt{v}=2$. The value calculated for Q ($Q=2Q_0$) was 2.53 cm^3/sec (152 cm^3 min^{-1}) giving a value for $\frac{r^4}{Q}=4.01\times10^{-3}$ cm sec.

Values for $\frac{I}{K}$ have been calculated from directly measured anemometer characteristics at measured currents for the anemometer of figure 6. At 12 mA current, $\frac{I}{K}$ has a value of 130 mV. (K has the dimensions of reciprocal ohms so that $\frac{I}{K}$ has the dimensions of milliampere ohms or millivolts.)

Assuming that $L=2h$ and combining all of the above estimates gives an overall estimated detector-sensitivity of 0.56×10^6 mV/g-cm^{-3}.

At a bridge current of 25 mA, a little over 50 mW is dissipated into and carried away by the reference gas. When the sample is absent, the heat is carried equally into each of the arms of the A branch, and, because of the vertical sections in the A branch, a certain amount of chimney effect is produced. When sample is present, the internal gas flow adds algebraically to the reference gas flow and the distribution of heat energy is changed, causing a change in the amount of chimney effect. The effect on the record of an eluted peak would be a failure to return promptly to zero, or to return to a displaced but reasonably constant zero because the effect of the changed heat distribution persists for some time after the sample has passed. For this reason, the amount of energy dissipated into the gas stream should be kept small, the reference gas ducts should be kept close together for some distance on both sides of the anemometers, and the mounting block should be made of a metal having a high thermal conductivity to minimize temperature differences.

From the above, it appears that the Nerheim gas density balance is affected by several design variables which, if properly chosen, can make it suitable for a number of applications involving either high or low sensitivity and large or small sample sizes. It is also subject to limitations which should be considered in its applications.

7. Appendix

Head loss coefficients for T-joints and 90° bends have been measured by a number of authors [8, 9, 10] at relatively high Reynolds numbers but actual measurements at low Reynolds numbers are scarce and none have been discovered which seem to apply to the conditions encountered in the gas density balance. Various schemes of extrapolation of the data into the laminar region have been proposed. Perhaps that of Prandtl [11] for use with 90° bends is the best known. The coefficient of resistance of the curved pipe, λ, is related to that of a straight pipe of the same length, λ_0, by the equation

$$\frac{\lambda}{\lambda_0} = 0.37\, D^{0.36}$$

in which D is the Dean number, $\frac{Re}{2}\left(\frac{r}{r_c}\right)^{1/2}$, with Re the Reynolds number and r_c and r, the radius of curvature and the pipe radius, respectively. This equation is reported [12] to apply between $10^{1.6} < Re\left(\frac{r}{r_c}\right)^{1/2} < 10^3$. However, at low Reynolds numbers and low values of

$\frac{r}{r_c}$ the ratio $\frac{\lambda}{\lambda_0}$ does not extrapolate to 1.0 as might be expected: e.g., at $Re=50$ and $\frac{r}{r_c}=100$, $\frac{\lambda}{\lambda_0}=0.51$. Walker, Lewis, McAdams, and Gilliland [13] give an empirical equation for estimating the loss coefficient K, for Reynolds numbers between 100 and 1000 and for $Re<10$, which does not include the range of interest here. However, using the data of Walker, et al., there has been developed [9] an expression which gives a practical estimate of losses in ordinary pipe fittings, T's and 90° elbows. Resistances to flow calculated for pipe fittings are probably somewhat greater than for similar joints in glass tubing, but will serve to give better than order-of-magnitude estimates on which to base the neglect or inclusion of such resistances in the A- and C-branch loop of figure 1.

The loss of head, h, in such pipe fittings as above is given in terms of the square of the velocity, V, the local acceleration of gravity, g, the friction factor, f, and the ratio of the length to diameter of the pipe, $\frac{L}{2r}$.

$$h=f\left(\frac{L}{2r}\right)\frac{V^2}{2g}$$

In the case of pipe T's and elbows it is customary to give a value of $\frac{L}{2r}$ which is larger, by some experimentally determined factor, than that for a straight section so that the head loss of the fitting is expressed as equivalent to a length of straight pipe in terms of its diameter. For laminar flow, the equivalent length, $\left(\frac{L}{2r}\right)_t$, of a fitting is given, to a good approximation, [9] in terms of its equivalent length for turbulent conditions, $\left(\frac{L}{2r}\right)_t$, by $\left(\frac{L}{2r}\right)_l=\frac{Re}{1000}\left(\frac{L}{2r}\right)_t$. The head loss for laminar flow, h_l, then becomes $h_l=f_l\frac{Re}{1000}\left(\frac{L}{2r}\right)_t\frac{V^2}{2g}$. The friction factor, f_l, for laminar flow is $\frac{64}{Re}$ so that $h_l=0.064\left(\frac{L}{2r}\right)_t\frac{V^2}{2g}$ or $h_l=K\frac{V^2}{2g}$. Values for $\left(\frac{L}{2r}\right)_t$ from reference [9] indicate that the bend resistance goes through a minimum at $r_c\cong 3.7r$, and approaches a maximum value of about 18 at $r_c\geq 36r$. For flow through the run of a T, $\left(\frac{L}{2r}\right)_t\cong 20$ and when the flow is through the branch $\left(\frac{L}{2r}\right)_t\cong 60$. The corresponding resistance coefficients are:

For 90° bends	$K_B=0.24$ minimum
For 90° bends	$K_B=1.15$ maximum
For T, through run	$K_r=1.28$
For T, through branch	$K_b=3.84$.

The head loss may be converted into resistance to flow, $\frac{\Delta P}{Q}$, by substituting $V=\frac{Q}{\pi r^2}$ and $\Delta P=\rho gh$ into the above so that resistance to flow through a fitting $=\frac{K}{2\pi^2r^4}\rho Q$. Summing the resistances for the bends and T's in the A- and C- branches and dividing by the total resistance, including the straight sections, the fraction of the total resistance due to the bends and T-joints becomes (assuming $\rho_1=\rho_2$)

$$\frac{\rho\left[K_r\left(\frac{3Q+Q_c}{2}\right)+K_bQ_c+K_BQ\right]}{16\pi\eta L+\rho\left[K_r\left(\frac{3Q+Q_c}{2}\right)+K_bQ_c+K_BQ\right]}$$

Reasonable values of the quantities in the above expression are as follows:

$\rho=1.1457\times10^{-3}$ g-cm^{-3} (N_2 at room temp. and 1 atm.)
$Q=150$ cm^3 min$^{-1}=2.5$ cm^3 sec^{-1}
$Q_c=25$ cm^3 min$^{-1}=0.417$ cm^3 sec^{-1}
$\eta=0.181\times10^{-3}$ poises (N_2 at room temp. and 1 atm.)

Substituting these values into the above and solving for the percentage of the total resistance which occurs in the T-joints and bends gives $L=\frac{120}{E}-1.2$ for the case where $r_c=36r$ and $L=\frac{91.5}{E}-0.92$ for $r_c=8r$, in which E is the error, in percent, caused by the neglect of bends and T-joints.

8. References

[1] Nerheim, A. G., Anal. Chem. **35,** 1640 (1963).
[2] Martin, A. J. P., U. S. Patent 2,728,219 (Dec. 27, 1955).
[3] Martin, A. J. P., and James, A. T., Biochem J., **63,** 138 (1956).
[4] Able, K., and Noble, F. W., Trans. N.Y. Acad. of Sci. Ser. II, **26** (No. 2) 159 (1963).
[5] Ower, E., The Measurement of Air Flow (Chapman and Hall Ltd., London, 1949).
[6] Haarhoff, P. C., and Vander Linde, H. J., Anal. Chem. **28,** 573–82 (1966).
[7] Guillemin, C. L., and Auricourt, A., J., Gas Chromatography **2,** 156–159 (1964).
[8] Beij, K. H., J. Res. NBS **21,** 1–18 (1938) RP1110.
[9] Flow of Fluids Through Valves Fittings and Pipe, Tech. Paper No. 410 (1965), Crane Co., Chicago.
[10] Ito, H., ASME Trans., Series D., J. Basic Eng. **82,** 131–143 (1960).
[11] Prandtl, L., Führer durch die Strömungslehre, 3d ed. p. 159, Braunschweig (1949).
[12] Schlichting, H., Boundary Layer Theory, p. 530 (McGraw-Hill Book Co., Inc., New York, N.Y., 1960).
[13] Walker, W. H., Lewis, W. K., McAdam, W. H., and Gilliland, E. R., Principles of Chemical Engineering (McGraw-Hill Book Co., Inc., New York, N.Y., 1937).

(Paper 72C3–276)

JOURNAL OF RESEARCH of the National Bureau of Standards—C. Engineering and Instrumentation
Vol. 72C, No. 2, July–September 1968

Standard Mismatch—the Production of Controlled Small Reflections in Waveguides*

L. Lewin**

(April 26, 1968)

The reflection properties of possible suitable structures, for producing small accurately controlled reflections in rectangular waveguide, are examined and a choice made of cylindrical posts for a more detailed study.

A number of sources of error due to ohmic loss, positioning and shape are investigated, and it is shown that both the inductive and capacitive post can meet reasonable specifications, but that the latter is the more suitable on almost all counts. Attention to post size and tilt is necessary, but the accuracies needed lie well within the range achievable by good engineering practice.

Key Words: Controlled small reflections; mismatch; reflector posts; waveguide.

List of Principal Symbols

a	rectangular waveguide broad dimension,
$\bar{\mathbf{a}}_x$, $\bar{\mathbf{a}}_y$	unit vectors,
b	rectangular waveguide narrow dimension,
d	post displacement from guide wall,
j	$(-1)^{1/2}$,
k	wave number in free space, $2\pi/\lambda$,
k'	wave number in waveguide, $2\pi/\lambda_g$,
r	post radius,
R	reflection coefficient,
T	transmission coefficient,
x	series reactance (normalized),
X	parallel reactance (normalized),
Z	post impedance (normalized),
δ, Δ	correction factors due to post conductance (see eqs (4) and (12)),
λ	free space wavelength,
λ_g	guide wavelength,
θ	post tilt angle, and
σ	post conductivity.

1. Introduction

The aim is to examine structures which can produce an accurately determined "standard" reflection in an otherwise matched rectangular waveguide. The voltage reflection level required is in the range 0.001 to 0.01. The structures should be simple and reliable to construct, be capable of being accurately calculated, and the uncertainties due to the unavoidable errors in assembly should be known within limits which ensure adequate maintenance of the expected reflections.

2. Possible Structures

There are, of course, an unlimited number of structures which could be contemplated for the purpose of producing a standard reflection of small magnitude. Almost any slight disturbances to the guide will suffice. Small perturbations can be accurately calculated, and provided they can be reliably made and measured, could form the basis of a standard reflection.

In order to keep this survey within reasonable bounds, a suitable selection from the possible forms must be made. We shall exclude all dielectric inserts on the grounds that, in addition to their geometry, an accurate figure for the dielectric constant needs to be known over a working temperature range. This makes such inserts possibly unsuitable as a standard.

The shapes which lend themselves readily to both calculation and to mechanical construction include inductive and capacitive rods and diaphragms. However, the diaphragm insert, in addition to requiring a correction for its finite thickness, has the complication that it contains two sharp edges. Since the sharpness can never be precisely defined, this makes it difficult to estimate errors arising from departures from a perfect geometrical form. Moreover, a very high current density flows at the sharp edges, making a possible loss contribution to be considered. For these reasons we will leave out the diaphragms from this survey.

We shall examine the inductive and capacitive rods in the next two sections.

*An invited paper.
**Present address: Standard Telecommunications Laboratories, Ltd., London Road, Harlow, Essex, England.

3. Inductive Rods

3.1. The Post Reactance

A rod of radius r is placed across the guide a distance d from one (narrow) guide wall as shown in figure 1. We are interested in small reflections, and therefore both d and r will be small. The dominant expression for the obstacle reactance X, which is connected with the reflection R by $R=-1/(1+j2X)$ is

$$X=\frac{a}{2\lambda_g}\operatorname{cosec}^2(\pi d/a)\{\log[(2a/\pi r)\sin(\pi d/a)] - \sin^2(\pi d/a)\cdot(2+k^2a^2/\pi^2)+k^2d^2[-\log(2\pi d/a) + 3/2+\pi^2d^2/36a^2]\} \quad (1)$$

This is eq (2.16)[1] of the publication cited in footnote 1 and is suitable for use for small d, giving large X and hence a small reflection. A more rigorous form is eq (2.14) [1] and a numerical calculation may be necessary in particular cases to confirm that eq (1) is sufficiently accurate.

3.2. Errors of Positioning

As an extremely crude, order of magnitude, approximation, eq (1) may be put in the form

$$X\simeq 1/(\pi d/a)^2 \quad (2)$$

which shows that R is proportional to d^2. An accurate placing of the rod is therefore necessary. To give $R=0.001$, we need $d\simeq a/100$. In a 2-in guide this gives $d=20$ mils; and a 1-mil error in placing gives rise to a 10 percent error in the reflection. This may seem large, though it is actually only a 0.0001 reflection, which is likely to be of the same order as effects due to other errors in the system. However, it seems undesirable to permit a 10 percent error, and either a more accurate construction is needed or else an alternative structure which is less sensitive to position. (Of course, jig-boring to a much better accuracy than 1 mil can be achieved if it is really required.)

When $R=0.01$, d is about three times larger, and the relative error in reflection is about 3 percent for a 1-mil positional error.

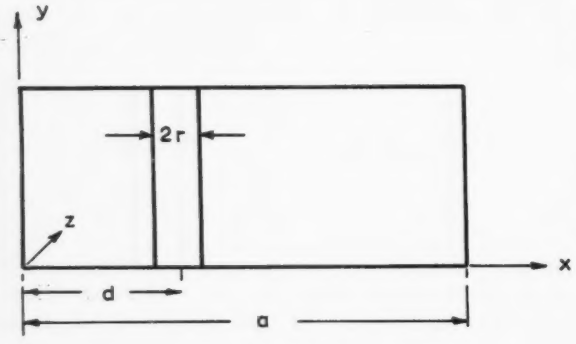

FIGURE 1. *Inductive post.*

3.3. Post Tilt

If the post is set at an angle θ to the normal, the effective field at the post is reduced by a factor $\cos\theta$, while its effect back into the guide is reduced by the same amount. An estimate of θ might be, for example, 1 mil in 1 in giving $\theta=10^{-3}$ rad, for which $\cos^2\theta$ differs insignificantly from unity.

In addition to this effect, a cross-component of electric field proportional to $\sin\theta$ will introduce a capacitive post effect, proportional to both $\sin^2\theta$ and the square of the post radius. This term is completely negligible.

3.4. Finite Post Radius

A higher-order correction to eq (1) is given by eq (2.43) of footnote 1. For small r and d the fractional correction is, very approximately, r^2/d^2. Thus if $d=20$ mils in a 2-in guide (to give a 0.001 reflection), the percentage error, if the wire radius is 5 mils, is about 7 percent. For a 0.01 reflection, d in this example is about 60 mils and an error of about 1 percent can be expected. If these errors are too great to be tolerated for a particular application, equation (2.43) should be used in preference to eq (1). It may also be desirable to use a somewhat larger wire diameter, in which case the more accurate formula should definitely be used.

3.5. Finite Post Resistivity

In appendix 1 it is shown that the effect of a conductivity σ for the post material leads to the normalized impedance of the post, jX, being augmented to

$$Z=(1+j)k'a/[8\pi kr\sin^2(\pi d/a)(30\lambda\sigma)^{1/2}]+jX \quad (3)$$

Since $X=0(1)/\sin^2(\pi d/a)$, the fractional correction due to finite conductivity can be estimated from the expression

$$\Delta=k'a/8\pi kr(30\lambda\sigma)^{1/2} \quad (4)$$

As an example to show the order of magnitude, take $r=1$ mm, $a=5$ cm, $\lambda=7.5$ cm, $\sigma=5.10^5$ mho/cm.

Then $\Delta\simeq 10^{-4}$, and the effect is completely negligible. The post radius would have to be quite minute for an effect to show up.

3.6. Conclusions for Inductive Post

Of the four possible causes of error considered, the effects of tilt and post resistivity are negligible. The corrected formula (2.43) (see footnote 1) for finite post radius should probably be used, in which case,

[1] Lewin, L., Advanced Theory of Waveguides, pp. 26, 27, 35, 44, and 77 (Iliffe and Sons, Ltd., London, 1951).

no error should occur from this source. Due to the rapid rise of the reflection as the post moves away from the side wall, a very accurate positioning is needed, but this should be within the bounds of good engineering practice. A possible further source of error can come from the contact where the post meets the guide. If this is soldered, the quality of the contact may not be known for certain, and possible further effects due to the extrusion of solder into the guide may occur. The latter may be avoided by using a technique in which the rods are very slightly oversize, are shrunk in liquid nitrogen, and then allowed to expand in situ. The uncertain effect of the contact resistance remains, however.

It is concluded that the inductive post is a possible but not ideal solution to the problem.

4. Capacitive Rods

4.1. The Post Reactance

Equations (2.74) and (2.75) (see footnote 1) give the series and parallel components of the equivalent circuit. (Note that k must be replaced by k'.) The formulas contain correction terms due to the finite post radius. Ignoring these for the moment, we have two equal series arms of normalized reactance magnitude

$$x = -\pi k' r^2/2b \tag{5}$$

and a parallel arm of magnitude

$$X = -b/(2\pi k' r^2) \tag{6}$$

The reflection and transmission coefficients are given by

$$jx = (1+R-T)/(1-R+T) \tag{7}$$

$$j(X+\tfrac{1}{2}x) = -\tfrac{1}{2} + 1/(1-T-R)$$

To terms in order r^2 this gives

$$R \simeq j[x + 1/(2X)] = -j3\pi k' r^2/2b \tag{8}$$

For example, if $b = 2.5$ cm, $\lambda = 7.5$ cm, then $r \simeq 1$ mm for a reflection of 0.01, and corresponding values proportional to r^2 for different radii.

4.2. Errors of Positioning

The formula quoted is for a central post, and therefore cannot be used for estimating positional errors. On general grounds, however, it can be said that if an obstacle is placed at a position d where the relevant mode has a magnitude $\Phi(d)$, then the variation of the reflection with d will involve $\Phi^2(d)$ as the dominant effect. This can be seen from eq (1), for example, where the factor $\text{cosec}^2\ (\pi d/a)$ in the reactance (which is inverted for the reflection coefficient) comes from $\Phi(d) = \sin\ (\pi d/a)$, the form of the dominant waveguide mode.

In the present case, the dominant mode is unvarying with d, since it is constant across the guide. Except for proximity effects when d is very small, there is no other variation. Hence, for a central post (and there seems no point in taking it off center), no errors of positioning need be expected.

4.3. Errors of Radius

Since $R \propto r^2$, we have, for small errors δr, δR

$$\delta R/R = 2\delta r/r. \tag{9}$$

An error of 1 mil in a 25 mil radius post gives a 4 percent reflection error. Since rods can certainly be turned to a much greater accuracy than this, errors due to incorrect post diameters can certainly be made negligible.

4.4. Finite Post Radius

The correction terms to eqs (5), (6), and (8) are of relative order $(k'r)^2$, or about 1 percent. This is probably negligible, but resort to the exact formulae in any particular case will give the correct reflection.

4.5. Finite Post Conductivity

As with the inductive post, the effect on rods of practical size is completely negligible.

4.6. Post Tilt

If the post is tilted at an angle θ, as shown in figure 2, a component of electric field proportional to $\sin\ \theta$ is set up along the post. This will excite the post as if it were in the inductive position, giving rise to a post current which will reradiate back into the guide by an amount containing a further factor $\sin\ \theta$. The analysis is given in appendix 2, where it is shown that an approximation to the reflection is

$$\delta R = \pi k b\ \sin^2\ \theta/[(k'b)^2\ \log\ (\pi r/2b)]. \tag{10}$$

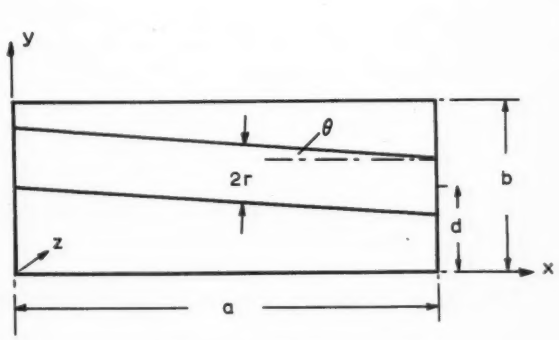

FIGURE 2. *Tilted capacitive post.*

If we take $b=2.5$ cm, $r=1$ mm, $\lambda=7.5$ cm, then

$$\delta R \simeq -\sin^2 \theta \tag{11}$$

An estimate of θ might be 2-mils error in 2 in, $\theta=10^{-3}$ radian and $\delta R=-10^{-6}$, and is only 0.1 percent of a reflection 0.001. We can therefore conclude that the effect of tilt can be made negligible.

4.7. Conclusions for Capacitive Post

Of the five possible causes of error, the effects of positioning and finite conductivity are completely negligible, while the effects of tilt, though potentially harmful, can be completely avoided by the achievement of the accuracy accompanying good engineering practice. The second-order corrections to the formulas, as given (see footnote 1), though probably negligible, can be readily calculated and allowed for.

The remaining source of error lies in the possible errors in machining the post diameter to size. The example used a 1-mil error in a 25-mil radius post, but it should be possible to achieve an order of magnitude better if it is really needed.

A possible source of error due to the post buckling has not been investigated, since this should not occur with a well engineered design. However, the axial (inductive post) effect should cancel to a first order for a symmetrical buckling, while the displacement effect should also be quite negligible.

Since no axial current flows in the capacitive post, the condition of the soldering at the ends seems to be a minor factor. The shrink-on process should be ideal here, though it would be as well to take precautions against buckling during the final expansion.

It is concluded that the capacitive post has all the requirements of a suitable low-reflecting obstacle—ease of accurate manufacture, absence of effects of positioning or other undesirable geometrical factors, absence of severe contact effects, and a fairly straightforward formula for the reflection. It also has the considerable advantage that undesirable higher-order modes are rapidly attenuated along the guide.

5. Conclusions

It is concluded that the central capacitive post is an almost ideal solution to the problem of achieving standard reflections in the 0.01 to 0.001 range, or, for that matter, over a more extended range.

This study was undertaken under the sponsorship of the Radio Standards Laboratory of the National Bureau of Standards.

6. Appendix 1. Effect of Finite Post Conductivity

The calculation proceeds almost exactly as stated in footnote 1 except that the boundary condition at the post, instead of being $E=0$ becomes

$$E=I(30/\lambda\sigma)^{1/2}(1+j)/r=I\delta, \tag{12}$$

(see eq (4.2) see footnote 1).

Instead of (2.10) we get

$$I=\sin(\pi d/a)\Big/\left[\delta+(60\pi jk/a)\sum_1^{\infty}\frac{\cos(m\pi r/a)-\cos(2m\pi d/a)}{\Gamma_m}\right] \tag{13}$$

Accordingly, the post impedance becomes

$$Z=jX+a\delta k'\ \operatorname{cosec}^2(\pi d/a)/240\pi k \tag{14}$$

where jX is the reactance for infinite conductivity. Equation (4) of the text follows directly.

7. Appendix 2. Effect of Tilt on Capacitive Post

We assume a capacitive post located across the guide at $y=d$, the guide being excited by a dominant mode of form $E_0 \sin(\pi x/a)\bar{a}_y$ at the post. If the post is tilted at a small angle θ from the perpendicular, a component of field will be produced along the post, of magnitude

$$E_0 \sin\theta \sin(\pi x/a)\bar{a}_x \tag{15}$$

This will cause radiation into the guide much as if the post were in the inductive position. We assume the field sets up a post current

$$i=I \sin(\pi x/a)\delta(z)\delta(y-d) \tag{16}$$

where I is a magnitude to be determined. The Hertzian vector has an x-component Π_x satisfying

$$\nabla^2\Pi_x+k^2\Pi_x=(120\pi j/k)I \sin(\pi x/a)\delta(z)\delta(y-d) \tag{17}$$

Assume $\Pi_x=\Pi \sin(\pi x/a)$ where Π is independent of x. Since $E=\operatorname{grad}\operatorname{div}(\mathbf{a}_x\Pi_x)+k^2\mathbf{a}_x\Pi_x$ we get, for the x-component of E, the equation $E_x=k'^2\Pi_x$, while $\nabla^2+k^2\equiv\partial^2/\partial y^2+\partial^2/\partial z^2+k'^2$. Hence

$$(\partial^2/\partial y^2+\partial^2/\partial z^2+k'^2)E_x = (120\pi jk'^2/k)I\delta(z)\delta(y-d)\sin(\pi x/a) \tag{18}$$

The solution to this equation is obtained as in reference [1], p. 25, giving

$$E_x=(-j120\pi k'^2/kb)I \sin(\pi x/a)\sum_1^{\infty}\sin\left(\frac{m\pi d}{b}\right)\sin\left(\frac{m\pi y}{b}\right)\frac{e^{-\Gamma_m|z|}}{\Gamma_m} \tag{19}$$

where $\Gamma_m = (m^2\pi^2/b^2 - k'^2)^{1/2}$. Equating this to the negative of the exciting field (eq 15) at $y = d + r$ determines I to give zero axial tangential field at the post surface.

$$I = \frac{E_0 \sin\theta\, kb}{60\pi j k'^2} \sum_1^\infty \frac{1}{\Gamma_m} [\cos(m\pi r/b) - \cos(2m\pi d/b)] \tag{20}$$

This current flows *along* the post, i.e., in the x direction. Due to the post tilt, a component $I \sin\theta$ reradiates back with polarization in the y direction. The formula for this radiation is given by eq (2.48) (see footnote 1), in which the dipole strength M is taken equal to $(-120\pi j/kb)I \sin\theta$. The dominant mode reradiated back into the guide comes from the first term in the series of modes of eq (2.48), from which the magnitude of the electric field is $(-60\pi/b)I \sin\theta$. Inserting for I from (20) gives the reflection due to the tilt

$$\delta R_{\text{tilt}} = \frac{-k \sin^2\theta}{k'^2 \sum_1^\infty \frac{1}{\Gamma_m} [\cos(m\pi r/b) - \cos(2m\pi d/b)]} \tag{21}$$

Taking $d = b/2$, this formula can be put in the approximate form, suitable for small r,

$$\delta R_{\text{tilt}} \doteq \frac{\pi \sin^2\theta\,(kb)}{(k'b)^2 \log(\pi r/2b)} \tag{22}$$

which is eq (10) of the text.

(Paper 72C3–277)

JOURNAL OF RESEARCH of the National Bureau of Standards—C. Engineering and Instrumentation
Vol. 72C, No. 3, July–September 1968

Viscoelastic Behavior of Dental Amalgam*

P. L. Oglesby, G. Dickson, M. L. Rodriguez,**
R. M. Davenport, and W. T. Sweeney

Institute for Materials Research, National Bureau of Standards, Washington, D.C. 20234

(April 12, 1968)

Measurements made on dental amalgam in tension indicate that amalgam exhibits three types of viscoelastic phenomena: (1) instantaneous elastic strain, (2) retarded elastic strain (transient creep), and (3) viscous strain (steady state creep). The combination of elastic plus retarded strain can be represented by an equation of the form $\epsilon = A\sigma + B^2\sigma^2$ where A and B are functions of time but not of the stress, σ. The viscous strain rate can be represented by an equation of the form $\dot{\epsilon}_v = K\sigma^m$ where K and m are constants of the material. By applying a nonlinear generalization of the Boltzmann superposition principle to a general equation describing the creep behavior of amalgam, the results of creep tests can be directly related to the results of stress-strain tests.

Key Words: Amalgam; creep; dental; steady-state creep; stress-strain; transient creep; viscoelastic.

1. Introduction

There is no information in the literature on the viscoelastic behavior of dental amalgam except the limited amount that can be obtained from stress-strain relationships [1, 2].[1] The stress-strain data indicate that amalgam exhibits a nonlinear relation between stress and strain over the entire range of stress investigated; this has been found to be true in both tension and compression. It has been further noted that the shapes of the stress-strain curves vary with the strain rate indicating that the strain developed is not only dependent on the applied stress but also upon time of application of the stress. The results of tensile stress-strain investigation by Rodriguez and Dickson [1] indicated that dental amalgam might be a viscoelastic material. It was, therefore, the objective of this study (1) to make an exploratory investigation of the types of viscoelastic phenomena exhibited by dental amalgam in tension, (2) to describe the viscoelastic phenomena exhibited by amalgam in terms of available viscoelastic theory and (3) to make available a practical example and method of application of viscoelastic theory to a dental material.

2. Theory

In general a strain-hardened material will exhibit one or more of three aspects of viscoelastic phenomena: (1) elastic behavior, (2) viscous behavior (steady-state creep), and (3) retarded elastic behavior (transient creep).

In a material which exhibits all three phenomena linearly related to the applied stress and in which the responses are additive (obey a superposition relation), the strain at any time may be represented by the equation

$$\epsilon = J_0\sigma + \sigma \int_0^\infty J'(\tau)(1-e^{-t/\tau})d\tau + \frac{\sigma t}{\eta}, \tag{1}$$

where

ϵ is the creep strain,
$J_0\sigma$ is the instantaneous elastic response,
$\sigma\int_0^\infty J'(\tau)(1-e^{-t/\tau})d\tau$ is the retarded elastic response,
$\frac{\sigma t}{\eta}$ is the viscous response,
σ is the applied stress,
J_0 is the elastic compliance, the reciprocal of the elastic modulus,
$J'(\tau)$ is a continuous distribution of retarded elastic compliances as a function of the variable retardation time τ of a continuous distribution of responses
t is the time after application of the stress, and
η is the coefficient of viscosity.

The relationship between creep strain and stress may not be linear as assumed above. For example, a

*This investigation is part of the dental research program conducted by the National Bureau of Standards in cooperation with the Council on Dental Research of the American Dental Association; the Army Dental Corps; the Dental Sciences Division of the School of Aerospace Medicine, USAF; the National Institute of Dental Research; and the Veterans Administration.

**Present address: Dental School, Loyola University, 6363 St. Charles Ave., New Orleans, Louisiana. 70118.

[1] Figures in brackets indicate the literature references at the end of this paper.

308-528 O - 68 - 2

material may obey the following equation:

$$\epsilon = J_0\sigma + \sigma \int_0^\infty J'(\tau)(1-e^{-t/\tau})d\tau$$

$$+\sigma^2\left[\int_0^\infty \beta(\gamma)(1-e^{-t/\gamma})d\gamma\right]^2 + K(\sigma-\sigma_0)^m t, \quad (2)$$

where $K(\sigma-\sigma_0)^m t = 0$ for all values of $\sigma \leq \sigma_0$ and

$\beta(\gamma)$ is a continuous distribution of retarded elastic compliances as a function of the variable retardation time γ of a continuous distribution of responses in the nonlinear second degree stress response of the material,

σ_0 is the applied stress level at which the material begins to exhibit a viscous flow, and

K and m are constants at any given temperature.

Where the creep strain is linearly related to the applied stress, the strain can be written as a product of a general creep compliance, which is a function of time only, and the applied stress as given by the following equation:

$$\epsilon = J(t)\sigma, \quad (3)$$

where

ϵ is the creep strain developed,
σ is the applied stress, and
$J(t)$ is the general creep compliance.

For example, in the linear creep behavior as seen in equation (1), the general creep compliance $J(t)$ is of the form:

$$J(t) = J_0 + \int_0^\infty J'(\tau)(1-e^{-t/\tau})d\tau + \frac{t}{\eta}. \quad (4)$$

In the case that creep strain is linearly related to the applied stress, the stress-strain behavior for a material may be related to the creep behavior by means of the linear superposition principle developed by Boltzmann [3] as shown below:

$$E(\sigma_t) = \int_0^{\sigma_t} J(T-\theta)d\sigma(\theta), \quad (5)$$

or

$$E(T) = \int_0^T J(T-\theta)\frac{d\sigma(\theta)}{d\theta}d\theta, \quad (6)$$

where

σ is the applied stress related to the experimental time θ in a prescribed experimental functional relation,

$E(T)$ is the strain of a stress-strain relation measured at a time T subsequent to the variable time θ, and

$\frac{d\sigma(\theta)}{d\theta}d\theta$ is the increment of stress from time θ to time $(\theta+d\theta)$.

For example, applying the Boltzmann superposition principle to the example of creep given in eq (1) gives the following relation between creep behavior and the strain measured in a stress-strain test [4]:

$$E(T) = J_0\sigma + \int_0^T \int_0^\infty J'(\tau)(1-e^{-\frac{(T-\theta)}{\tau}})d\tau \frac{d\sigma(\theta)}{d\theta}d\theta$$

$$+\int_0^T \frac{\sigma(\theta)}{\eta}d\theta. \quad (7)$$

A discussion of the application of the Boltzmann superposition principle as applied to linear viscoelastic phenomena is given by Leaderman [5]. However, if a material exhibits a nonlinear relation in its retarded strain (transient creep) and the applied stress, as discussed earlier, the linear Boltzmann superposition principle cannot be applied to relate strain of a stress-strain test on the material to the creep strain. A generalization of Boltzmann's superposition principle developed by Nakada [6] may be used to relate nonlinear retarded elastic creep behavior to the stress-strain behavior of the material as given:

$$E_R(\sigma) = \int_0^{\sigma(T)} \Psi(T-\theta)d\sigma(\theta) +$$

$$\int_0^{\sigma(T)}\int_0^{\sigma(T)} \Phi(T-\theta, T-\phi)d\sigma(\theta)d\sigma(\phi)$$

$$+\int_0^{\sigma(T)}\int_0^{\sigma(T)}\int_0^{\sigma(T)} F(T-\theta,$$

$$T-\phi, T-\alpha)d\sigma(\theta)d\sigma(\phi)d\sigma(\alpha) + \ldots \quad (8)$$

Now for example, consider the application of the nonlinear superposition principle of Nakada as applied to the case of retarded strain (transient creep) related to the applied stress by a second degree equation as shown earlier:

$$\epsilon_R = \sigma\Psi(t) + \sigma^2\Phi^2(t) \quad (9)$$

where $\Psi(t)$ and $\Phi(t)$ could be represented by the equation shown below in accordance with the Voigt model

$$\Psi(t) = \int_0^\infty J'(\tau)(1-e^{-t/\tau})d\tau,$$

$$\Phi(t) = \int_0^\infty \beta(\gamma)(1-e^{-t/\gamma})d\gamma.$$

If one applies an approximation of Nakada's general formulation described by Leaderman, McCrackin, and Nakada [7], the equation representing the retarded elastic response takes the following form:

$$E_R(\sigma(T)) = \int_0^{\sigma(T)} \Psi(T-\theta)d\sigma(\theta)$$

$$+\int_0^{\sigma(T)}\int_0^{\sigma(T)}\Phi(T-\theta)\Phi(T-\phi)d\sigma(\theta)d\sigma(\phi). \quad (10)$$

Considering an example of a material which exhibits all three phenomena but in which the creep strain is a nonlinear function of the applied stress according to eq (2), then applying the above approximation of the nonlinear superposition principle, the stress-strain behavior of the material may be related to the creep behavior by the following equation:

$$E=\sigma J_0+\int_0^T \Psi(T-\theta)d\sigma(\theta)$$

$$+\int_0^T\int_0^T \Phi(T-\theta)\Phi(T-\phi)d\sigma(\theta)d\sigma(\phi)$$

$$+\int_0^T K(\sigma(\theta)-\sigma_0)^m d\theta. \quad (11)$$

However, as will be discussed later, it was found in the investigation that a different approximation is required to describe the behavior of dental amalgam.

3. Materials

The specimens were prepared using a commercial alloy for dental amalgam certified to comply with American Dental Association Specification No. 1. This alloy (composition approximately Ag 70%, Sn 26%, Cu 3.5%, Zn 0.5%) was mixed with mercury and condensed into a mold as described by Rodriguez and Dickson [1] to produce a specimen with dimensions as shown in figure 1. Specimens were aged for at least one week to obtain essentially full mechanical strength [8].

4. Procedure

The dumbbell-shaped specimen was placed in the grips and Tuckerman optical strain gages were mounted on opposite sides of the specimen as shown in figure 2. To obtain the creep curve, readings were taken on the strain gages, a weight was suspended from the lower grip and a second strain gage reading was taken immediately. Strain readings were then made at 15 s intervals for 4 min and at increasingly longer intervals until the strain rate became constant (usually after approximately 1.5 hr). At the end of this period, the load was removed, a strain reading was taken immediately and the recovery curve was followed by reading first at 15 s intervals and then at longer intervals until the strain became constant.

Strain readings obtained on the two sides of the specimen were averaged and strain was plotted against time to obtain the loaded creep and unloaded recovery curves. Readings on the strain gages were normally made to the nearest 2×10^{-5} in. Since a gage length of 0.25 in was used this is equivalent to a strain of 8×10^{-5}. Thus, in the results given below, differences in strain of 1×10^{-4} are approximately equal to the minimum reading difference.

Loads placed on the specimen (with a nominal 0.01 in^2 cross-sectional area) varied from 5 to 40 lb giving stresses from approximately 500 to 4,000 psi. Most specimens were used for several runs, first at high and then at lower stresses. The first loaded creep run was considered a strain hardening treatment and data obtained on these runs were not used in the calculation of results other than for viscous strain rate. All runs were made at 23 ± 1 °C.

5. Results and Discussion

The creep curves (both loaded and recovery curves) of strain hardened dental amalgam as shown for a

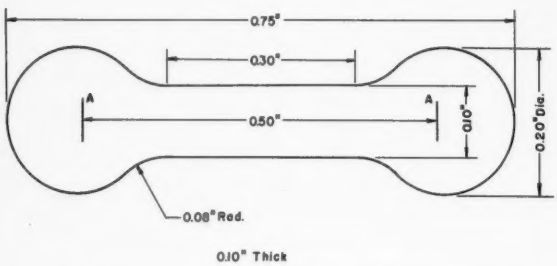

FIGURE 1. *Dimensions of the dumbbell-shaped tensile specimen of amalgam.*

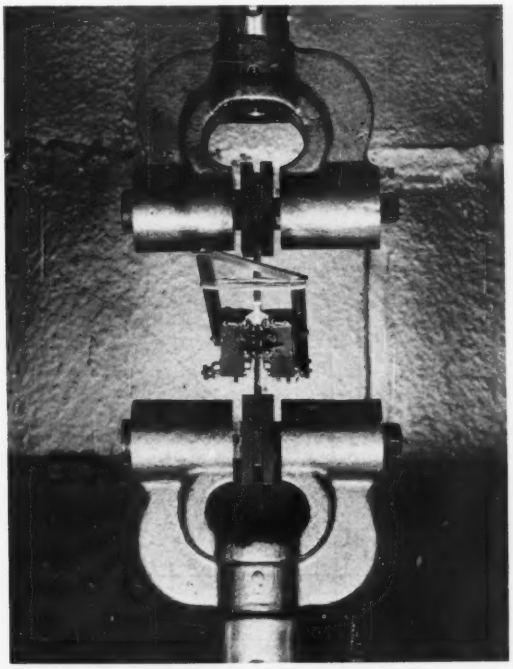

FIGURE 2. *Tensile specimen in position for load application with optical strain gages mounted on opposite sides of the specimen.*

number of different stress levels in figure 3 indicate that at room temperature amalgam exhibits three different types of viscoelastic phenomena: (1) instantaneous elastic strain, (2) retarded elastic strain (transient creep), and (3) viscous strain (steady-state creep).

The viscous strain rate was determined from the loaded portion of the creep curve by taking the slope of the straight line portion of the curve, and was also determined from the recovery portion of the creep curve by dividing the value of the recovery strain (the permanent strain in the specimen) by the total time the load was on the specimen. The viscous strain rates for any given creep curve as calculated from the loaded and recovery portions of the curve were found to agree fairly well as shown in table 1. The log of the viscous strain rate was found to be a linear function of the log of the applied stress, as shown in figure 4; thus the viscous strain rate could be related to the applied stress by the following equation:

$$\dot{\epsilon}_v = K\sigma^m, \qquad 12)$$

where

$\dot{\epsilon}_v$ is the viscous strain rate,
σ is the applied stress, and
K and m are constants of the material.

The value of m for amalgam is the value of the slope of the curve in figure 4, while the value of K is the antilog of the viscous strain rate value at a value of applied stress σ of 1 psi. For the dental amalgam used in this investigation values for K of 2.85×10^{-19} and 4.98×10^{-19} were obtained from loaded and unloaded data respectively, and values of 3.99 and 3.92 were obtained for m.

The strain developed in amalgam due to the other two phenomena (1) instantaneous elastic strain and (2) retarded strain can be determined from the strain recovery since these two types of strain are recoverable while the viscous strain is not. Thus, at any given load the strain values taken from the creep curve after the sample has been unloaded (that is in the recovery portion of the creep curve) are subtracted from the strain value on the creep curve at the instant just before unloading of the specimen. This difference is plotted against recovery time $t_i = T_i - T_u$ where T_u is the time at which the specimen was unloaded and

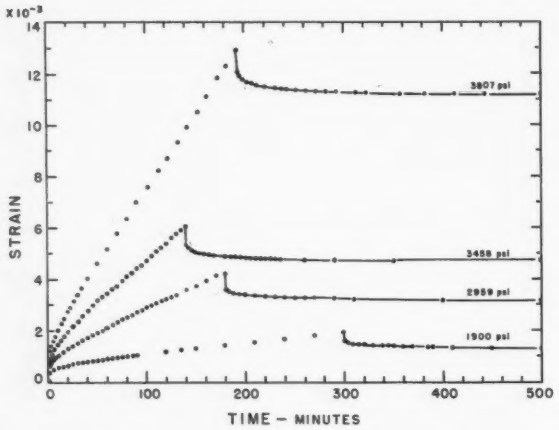

FIGURE 3. *Creep and recovery of amalgam loaded in tension.*

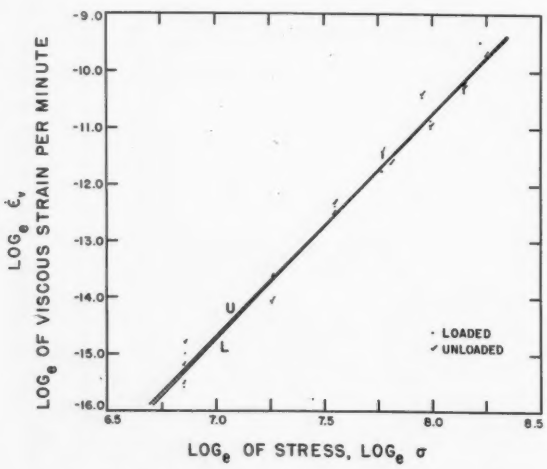

FIGURE 4. *Relationships between viscous strain rate and stress.*

Straight lines are least-squares fits of equation $\log \dot{\epsilon}_v = \log K + m \log \sigma$ to the data, with errors assumed to be in $\log \dot{\epsilon}_v$ only. Loaded values are from straight portion of creep curve; unloaded values are from strain remaining in specimen after unloading and recovery.

TABLE 1. *Viscous strain rates*

Specimen–run	Stress lb/in.^{2}	Strain per minute	
		Loaded $\times 10^{-5}$ [a]	Unloaded $\times 10^{-5}$ [b]
41–40–1	3807	5.65	[c] 6.35
41–40–2	3807	5.98	5.80
39–40–1	3731	4.92	[c] 5.74
39–40–2	3731	5.23	5.08
40–40–1	3731	7.45	[c] 8.04
43–35–1	3458	3.12	[c] 3.71
43–35–2	3458	3.23	3 28
43–35–3	3458	3.42	3.44
44–30–1	2959	1.92	[c] 1.98
44–30–2	2959	1.68	1.68
44–30–3	2959	1.74	1.72
41–30–3	2855	2.84	2.96
44–25–4	2465	0.91	0.89
35–25–1	2375	1.05	[c] 1.33
35–25–2	2375	0.98	1.06
35–25–3	2375	1.03	1.08
38–25–1	2366	1.09	[c] 1.40
38–25–2	2366	0.783	0.821
38–25–3	2366	.785	.806
35–20–4	1900	.384	.....
35–20–5	1900	.419	0.435
38–20–4	1892	.349	.358
35–15–6	1425	.111	.113
38–15–5	1419	.076	.077
35–10–7	950	.031	.034
38–10–6	946	.023	.025
38–10–7	946	.017	.018
35–05–8	475	.008	.007

[a] From slope of straight portion of loaded creep curve.
[b] From strain remaining in specimen after unloading and recovery.
[c] These values include effects of strain hardening and were not used in calculating the relation between stress and viscous strain rate.

T_i is the time of the strain value on the recovery portion of the curve. These difference values, ϵ', are seen plotted against the recovery time for each load or stress in figure 5. These plots are a measure of the combination of the elastic and retarded elastic strain behavior of dental amalgam as a function of time for various stress levels. A measure of the combination of elastic and retarded strain may also be obtained from the loaded portion of the creep curve by taking values off the loaded creep curve and subtracting the viscous strain accumulated in the specimen at that time. The accumulated viscous strain at any time may be calculated by multiplying the viscous strain rate by the time corresponding to that value on the creep curve. Thus the difference between the creep curve value on the loaded portion and the viscous strain value at a corresponding time is a measure of the combination of the instantaneous and retarded elastic strain. However, a small error in the viscous strain rate causes a large error in the difference value. Therefore, the plot of the combination of elastic and retarded elastic strain versus time as obtained from the loaded creep curve is subject to large possible error.

Using the approximation of Nakada's general formulation described by Leaderman, McCrackin, and Nakada [7], the ordinates of the inverted recovery curves as described above should be greater in the early portion of the time scale than the ordinates of the loaded portion of the creep curves minus the viscous strain. The difference between the curves should rise to a maximum within the first few minutes and gradually decrease to zero as time increases. However, as shown in figure 6, the loaded curves appear to lie above the recovery curves. Fitting such data to Nakada's formulation would be very difficult. Moreover, the differences are not large and the method of obtaining values for the loaded curves is subject to considerable error because the loaded curves had to be corrected by subtracting the viscous component. Thus it is believed that the differences between the curves are not significant and so the curves were treated as though they are superimposable. Therefore, the data reported for the combination of elastic and retarded elastic strain were obtained from the recovery portion of the creep curves.

The combination elastic strain (instantaneous and retarded elastic strain) becomes asymptotic with time in accordance with theory as seen in figure 5. The combination elastic strain values were plotted as a function of the various stress levels for corresponding time, as shown in figure 7. The combination elastic strain is seen to be a nonlinear function of the applied stress. When the combination strain values were divided by their corresponding stresses and then plotted against the corresponding stress for a fixed time, a linear plot was obtained for each fixed time as illustrated in figure 8; this result indicated that the combination elastic behavior of amalgam as a function of applied stress under the test conditions could be represented by an equation of the form:

$$\epsilon' = A(t)\sigma + B^2(t)\sigma^2, \tag{13}$$

where

ϵ' is the combination of elastic and retarded elastic strain, and
σ is the applied stress.

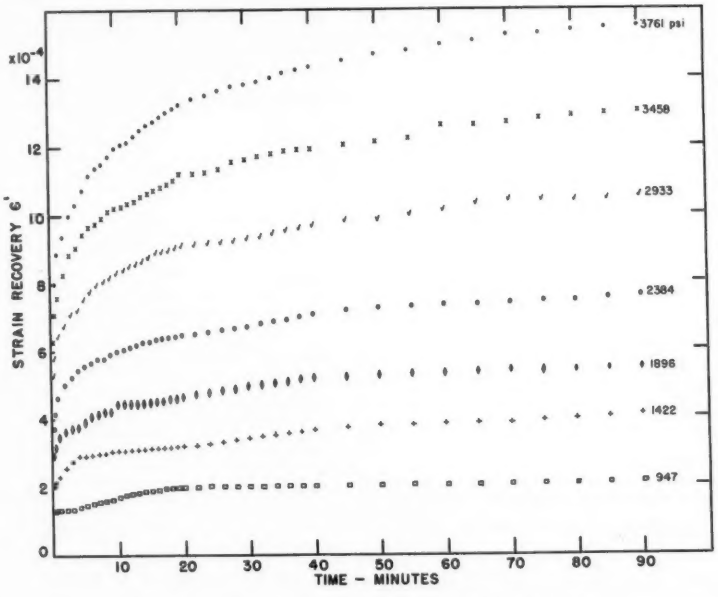

FIGURE 5. *Strain recovery after release of tensile stress.*
Each curve is an average of 2 to 7 runs.

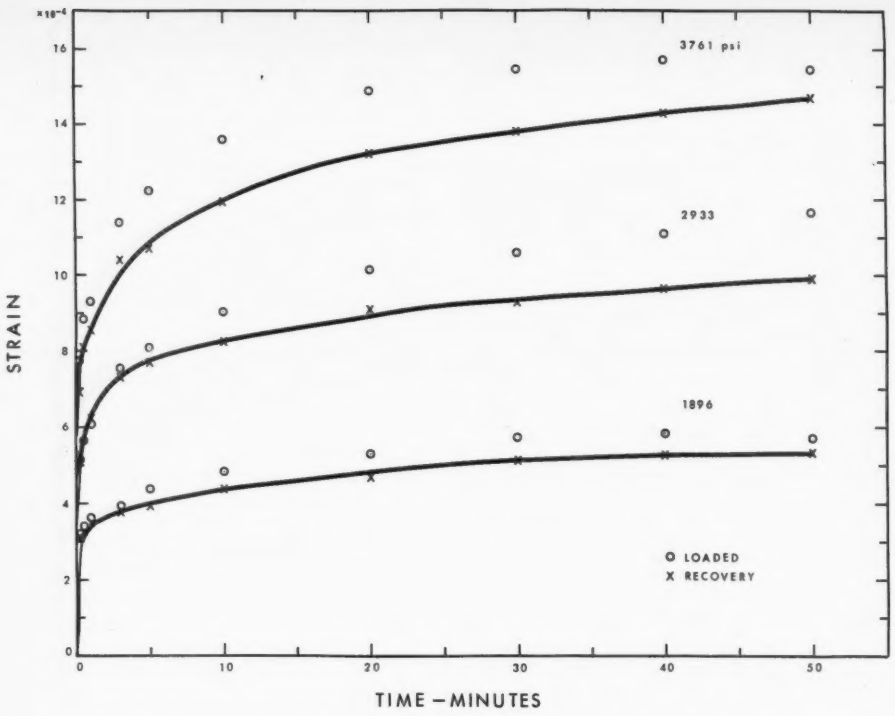

FIGURE 6. *Comparison of inverted recovery curves with loaded creep curves minus the viscous strain.*

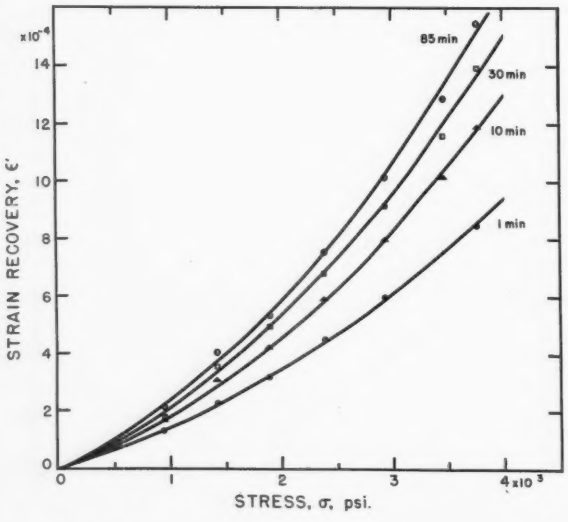

FIGURE 7. *Relationships between recovery strain, stress and time.*

Plotted points are averages of 2 to 7 determinations. Curves are calculated from least-squares fits of the equation $\epsilon'/\sigma = A(t) + B^2(t)\sigma$ to the data with error assumed to be in ϵ'/σ only.

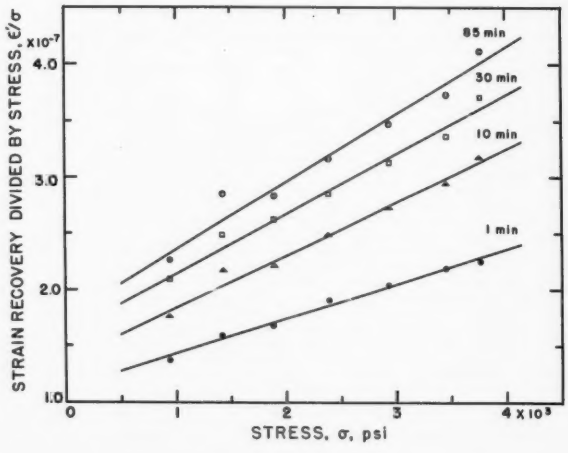

FIGURE 8. *Relationships between recovery strain, stress and time.*

Plotted points are averages of 2 to 7 determinations. Straight lines represent the constants obtained by least-squares fit of the equation $\epsilon'/\sigma = A(t) + B^2(t)\sigma$ to the data with error assumed to be in ϵ'/σ only.

$A(t)$ and $B^2(t)$ are functions[2] of time but not of stress. The value of $A(t)$ for any time value is the intercept at $\sigma=0$ of the plot for that time value as shown in figure 8 while $B^2(t)$ is the slope of the straight line for that time value. It is also noted in figure 8 that as a function of stress the combination strain divided by the stress is a straight line for all values of t. This indicated that over all ranges of t, the combination elastic strain obeys the same functional relation to the stress. Since the recovery curves were found to be superimposable upon the loading curves minus the viscous portion, it appeared that the nonlinear material did not obey the approximation of nonlinear generalization previously noted [7]. It was then questioned whether the retarded behavior of amalgam was truly nonlinear or whether the nonlinear behavior could be attributed to the geometry of the specimen being observed. However, longer specimens were tested and found to give the same result, also photoelastic specimens were made and the stress distribution over the area observed was found to be uniform. It is therefore concluded that the observed nonlinear behavior of dental amalgam is not a geometric artifact, but an intrinsic phenomenon in the material. The difference between the recovery curves and the loading curves minus the viscous portion is given by [7]:

$$2\sigma_0^2[\Phi(\Delta T, T)-\Phi(T, T)],$$

where ΔT is the time the specimen was under the load σ_0. For amalgam, this difference is found to be zero, so:

$$\Phi(\Delta T, T)=\Phi(T, T) \tag{14}$$

for creep recovery from equilibrium, i.e., for ΔT large. McCrackin [9] has suggested that this condition be satisfied by assuming that the value of Φ is only dependent on the value of the least of its arguments. That is,

$$\Phi(T_1, T_2)=B^2(T_1) \text{ if } T_1 \leq T_2. \tag{15}$$

With this condition, the quadratic term of eq (8) is shown in the Appendix to reduce to

$$\int_0^{\sigma(T)} B^2(T-\theta)d[\sigma^2(\theta)] \tag{16}$$

so, eq (8) reduces to:

$$E_R(T)=\int_0^{\sigma(T)} A(T-\theta)d\sigma(\theta) + \int_0^{\sigma(T)} B^2(T-\theta)d[\sigma^2(\theta)]. \tag{17}$$

[2] The notation $B^2(t)$ rather than $B(t)$ is used for consistency with the form of the notation of Leaderman, McCrackin, and Nakada [7].

TABLE 2. *Values of* A(t) *and* $B^2(t)$ *in equation* $\epsilon' = A(t)\sigma + B^2(t)\sigma^2$

Time – min	$A(t) \times 10^{-7}$	$B^2(t) \times 10^{-11}$
0.25	1.130	1.906
.50	1.120	2.468
1.00	1.132	3.065
2.00	1.183	3.548
3.00	1.206	3.876
5.00	1.248	4.285
10.00	1.356	4.737
20.00	1.518	5.100
30.00	1.598	5.364
40.00	1.626	5.636
50.00	1.648	5.839
60.00	1.668	5.970
70.00	1.693	6.031
80.00	1.727	6.050
90.00	1.761	6.064
120.00	1.812	6.223
150.00	1.877	6.224
200.00	1.952	6.210
300.00	2.074	6.082
600.00	2.103	6.290
1000.00	2.079	6.497

ϵ' is combination of instantaneous and retarded elastic strain.
σ is stress.
$A(t)$ and $B^2(t)$ are constants for any time and are functions of time but not of stress.

The values for $A(t)$ and $B^2(t)$ were determined by fitting curves to the data by the method of least squares and were tabulated as a function of time as shown in table 2.[3] The $A(t)$ values were plotted as a function of the corresponding t values as shown in figure 9. The $A(t)$ values are seen to approach an asymptote, A_{as} as $t \to \infty$. Thus, the curve as shown in figure 9 could be represented by the following equation from linear viscoelastic theory since $A(t)$ is the linear term in stress:

$$A(t)=J_0+\int_0^{\infty} J'(\tau)(1-e^{-t/\tau})d\tau, \tag{18}$$

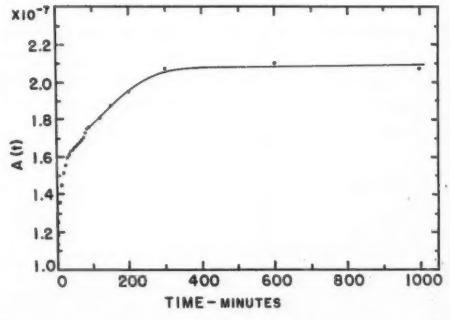

FIGURE 9. *Variation with time of the linear creep compliance term,* A(t), *in the equation* $\epsilon' = A(t)\sigma + B^2(t)\sigma^2$.

[3] Strain values for different stresses were obtained at each of the specific times listed in table 2 (and for many other times not listed in the table) by interpolation between the recorded values of strain along each of the 25 to 30 creep and recovery curves. Then the strain values for a specific time were fitted to the equation $\epsilon'/\sigma = A(t) + B^2(t)\sigma$ to obtain the values of $A(t)$ and $B^2(t)$ for that specific time.

$$A(t) = J_0 + \int_0^\infty J'(\tau)d\tau - \int_0^\infty J'(\tau)e^{-t/\tau}d\tau, \quad (19)$$

$$A(t) = A_{as} - \int_0^\infty J'(\tau)e^{-t/\tau}d\tau, \quad (20)$$

$$A_{as} - A(t) = \int_0^\infty J'(\tau)e^{-t/\tau}d\tau, \quad (21)$$

where

$A(t)$ is the creep compliance term which is linear in stress,
J_0 is instantaneous elastic compliance,
$J'(\tau)$ is the retarded elastic compliance spectrum as a function of the retardation time τ, and
A_{as} is the asymptote value of $A(t)$ as t becomes very large.

Thus, eq (20) does describe the behavior of $A(t)$ as a function of time as seen in figure 9. The linear creep compliance term $A(t)$ is plotted as a function of log t to obtain a signoidal curve as shown in figure 10. The first plateau of the signoidal plot at very small values of t should correspond to J_0 (the instantaneous elastic compliance) [10]. The value of J_0 calculated from the curve is 1.13×10^{-7} in^2/lb, equivalent to a modulus of elasticity of 8.9×10^6 lb/in^2. This value is in good agreement with a value of 9.1×10^6 reported for the modulus of dental amalgam determined by an ultrasonic method [11].

The nonlinear creep compliance term $B^2(t)$ was plotted against log t to obtain a sigmoidal curve as shown in figure 11. Thus, in the nonlinear theory of Nakada [6] the experimental $B(t)$ for amalgam might be represented by the following equation:

$$B(t) = \sqrt{B^2(t)} = \int_0^\infty \beta(\gamma)(1 - e^{-t/\gamma})d\gamma \quad (22)$$

which would indeed describe the behavior of the curves seen in figure 11. The combination elastic behavior of dental amalgam in creep under the test conditions used could then be described by means of the following equation from viscoelastic theory [6, 10]:

$$\epsilon' = A(t)\sigma + B^2(t)\sigma^2,$$

$$\epsilon' = J_0\sigma + \sigma\int_0^\infty J'(\tau)(1 - e^{-t/\tau})d\tau + \left[\int_0^\infty \beta(\gamma)(1 - e^{-t/\gamma})d\gamma\right]^2 \sigma^2. \quad (24)$$

and since the loaded portion of the creep curve for amalgam is also composed of viscous strain ϵ_v as well as combination elastic strain ϵ' then the strain on the loaded portion is composed of the sum of the two

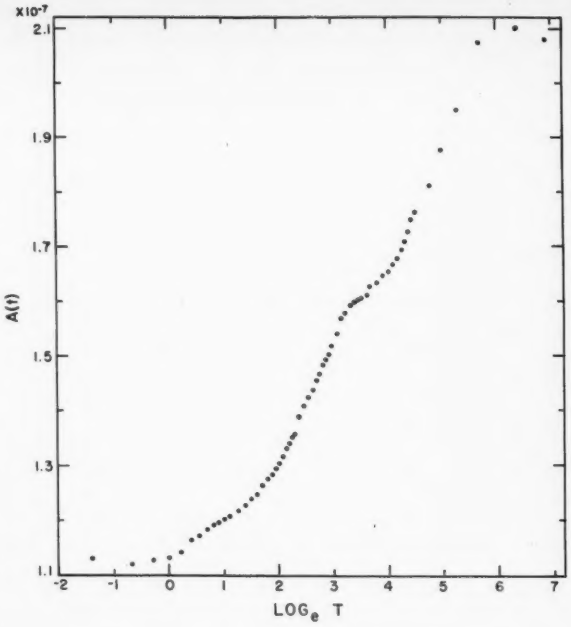

FIGURE 10. *Variation with log of time of the linear creep compliance term,* A(t), *in the equation* $\epsilon' = A(t)\sigma + B^2(t)\sigma^2$.

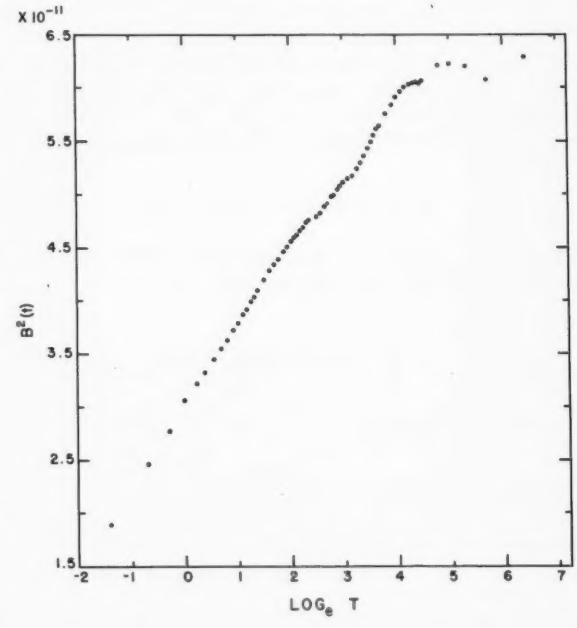

FIGURE 11. *Variation with log of time of nonlinear creep compliance term,* $B^2(t)$, *in the equation* $\epsilon' = A(t)\sigma + B^2(t)\sigma^2$.

as follows:

$$\epsilon = \epsilon' + \epsilon_p. \tag{25}$$

Thus

$$\epsilon = J_0\sigma + \sigma\int_0^\infty J'(\tau)(1-e^{-t/\tau})\,d\tau + \left[\int_0^\infty \beta(\gamma)(1-e^{-t/\gamma})\,d\gamma\right]^2 \sigma^2 + K\sigma^m t. \tag{26}$$

Therefore, applying both linear and nonlinear viscoelastic theory to the experimental behavior of amalgam under the test conditions used, a general equation describing the creep behavior of amalgam as given by eq (26) above is obtained.

Applying the nonlinear generalization of the Boltzmann superposition principle as developed by Nakada [6], to the above creep equation for amalgam, the stress-strain curves for various stress rate conditions were calculated for amalgam from the creep data and compared to the experimental stress-strain curves obtained under those conditions. The stress-strain curve corresponding to the experimental stress rate was calculated from the following equation:

$$E_T(n\Delta t) = \sum_{i=1}^{n} (\sigma_i - \sigma_{i-1})\left(\frac{A_{n-1} + A_{n+1-i}}{2}\right) + \sum_{i=1}^{n} (\sigma_i^2 - \sigma_{i-1}^2)\left(\frac{B_{n-1}^2 + B_{n+1-i}^2}{2}\right) + \Delta t \sum_{i=1}^{n} K\left(\frac{\sigma_{i-1} + \sigma_i}{2}\right)^m \tag{27}$$

which is a finite difference approximation to eqs (17) and (12). For the experimental data, the testing machine was run at a constant head speed which produced a varying stress rate over a total time of 3½ min. From the stress versus time curve, observed stress values were obtained at 15-s intervals. Using the values of $A(t)$ and $B(t)$ calculated for 15-s intervals from the creep data and also the viscous constants from these data, a curve was calculated for comparison with the experimental curve. Figure 12 shows the contribution of instantaneous elastic, retarded elastic and viscous components to the total calculated strain. It is seen in figure 13 that good agreement is obtained between the calculated and experimental stress-strain curves. Thus, it is concluded that in the case of dental amalgam the results of creep tests can be related to those of stress-strain tests by use of viscoelastic theory [6, 10].

6. Conclusion

Dental amalgam was found to exhibit three types of viscoelastic phenomena: (1) instantaneous elastic strain, (2) retarded elastic strain (transient creep), and (3) viscous strain (steady state creep).

The combination of elastic plus retarded strain in tension was found to be a nonlinear function of

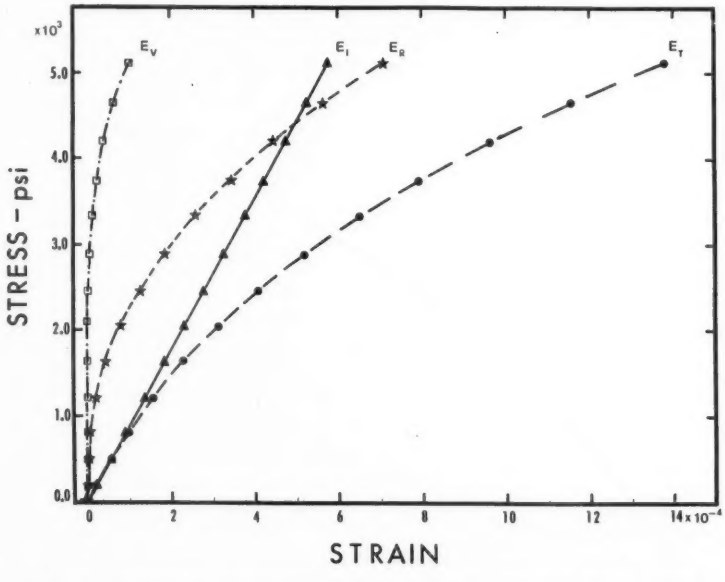

FIGURE 12. *Calculated instantaneous elastic strain* E_I, *retarded elastic strain* E_R, *viscous strain* E_V, *and total strain* E_T *occurring during a stress-strain test of dental amalgam.*

Head speed of testing machine was constant, and total time was 3½ min.

stress and could be represented by an equation of the following form:

$\epsilon' = A\sigma + B^2\sigma^2$ where A and B are functions of time, but not of stress.

The viscous strain rate is also a nonlinear function of stress and can be represented by an equation of the form:

$\epsilon_v = K\sigma^m$ where K and m are constants of the material.

An equation describing the creep behavior of amalgam was obtained by the application of nonlinear viscoelastic theory to the experimental behavior of amalgam under the test conditions used. By applying the nonlinear generalization of the Boltzmann superposition principle to this equation the results of creep tests were related to results of stress-strain tests.

7. Appendix

The derivation of eq (16) is as follows [9]:

$$\int_0^{\sigma(T)} \int_0^{\sigma(T)} \Phi(T-\theta, T-\phi)\, d\sigma(\theta)\, d\sigma(\phi)$$

$$= \int_0^{\sigma(T)} \int_0^{\sigma(\theta)} B^2(T-\theta)\, d\sigma(\phi)\, d\sigma(\theta)$$

$$+ \int_0^{\sigma(T)} \int_{\sigma(\theta)}^{\sigma(T)} B^2(T-\phi)\, d\sigma(\phi)\, d\sigma(\theta).$$

The first integral is

$$\int_0^{\sigma(T)} B^2(T-\theta) \left[\int_0^{\sigma(\theta)} d\sigma(\phi) \right] d\sigma(\theta)$$

$$= \int_0^{\sigma(T)} B^2(T-\theta)\sigma(\theta)\, d\sigma(\theta)$$

$$= \frac{1}{2} \int_0^{\sigma(T)} B^2(T-\theta)\, d[\sigma^2(\theta)].$$

Applying Dirichlet's formula [12] to the second integral,

$$\int_{\theta=0}^{T} \left[\int_{\phi=\theta}^{T} B^2(T-\phi) \frac{d\sigma(\phi)}{d\phi} \frac{d\sigma(\theta)}{d\theta}\, d\phi \right] d\theta$$

gives

$$\int_{\phi=0}^{T} \left[\int_0^{\phi} B^2(T-\phi) \frac{d\sigma(\phi)}{d\phi} \frac{d\sigma(\theta)}{d\theta}\, d\theta \right] d\phi$$

$$= \int_0^T \left[B^2(T-\phi) \frac{d\sigma(\phi)}{d\phi} \int_0^{\phi} \frac{d\sigma(\theta)}{d\theta}\, d\theta \right] d\phi$$

$$= \int_0^T B^2(T-\phi) \frac{d\sigma(\phi)}{d\phi} \sigma(\phi)\, d\phi$$

$$= \frac{1}{2} \int_0^T B^2(T-\phi) \frac{d[\sigma^2(\phi)]}{d\phi}\, d\phi.$$

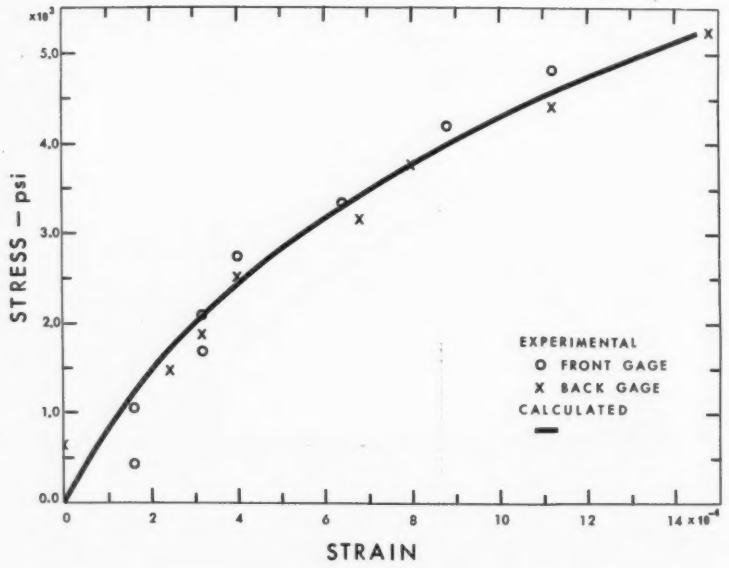

FIGURE 13. *Comparison of calculated and experimental stress-strain curves.*

However, this is the same as the first integral as θ and ϕ are dummy variables of integration so the sum of the integrals is

$$\int_0^T B^2(T-\theta)\frac{d[\sigma^2(\theta)]}{d\theta}d\theta=\int_0^{\sigma(T)} B^2(T-\theta)d[\sigma^2(\theta)].$$

8. References

[1] Rodriguez, M. L., and Dickson, G., J. Dental Research **28,** 441 (1962).

[2] Smith, D. L., Caul, H. J., and Sweeney, W. T., J.A.D.A. **53** 677 (1956).

[3] Boltzmann, L., Sitzber, Kgl. Akad. Wiss Wien. **70,** 275 (1874).

[4] Bland, D. R., The Theory of Linear Viscoelasticity (Pergamon Press, N.Y., 1960).

[5] Leaderman, H., Elastic and Creep Properties of Filamentous Materials and Other High Polymers. Textile Foundation, Washington, D.C. (1943).

[6] Nakada, O., J. Phys. Soc. Japan **15,** 2280 (1960).

[7] Leaderman, H., McCrackin, F., and Nakada, O., Trans. Soc. Rheology **7,** 111 (1963).

[8] Ryge, G., Dickson, G., Smith, D. L., and Schoonover, I. C., J.A.D.A. **45,** 269 (1952).

[9] McCrackin, F., Polymers Division, National Bureau of Standards, personal communication.

[10] Leaderman, H., Rheology **2,** p. 14 (Academic Press, Inc., N.Y., 1958).

[11] Dickson, G., and Oglesby, P. L., J. Dental Research **46,** 1475 (1967).

[12] Widder, D. V., Advanced Calculus (Prentice Hall, Inc., 1947).

(Paper 72C3–278)

JOURNAL OF RESEARCH of the National Bureau of Standards—C. Engineering and Instrumentation
Vol. 72C, No. 3, July–September 1968

The Steady-State Creep Behavior of Dental Amalgam*

George Dickson, Philip Oglesby, and Ruth Davenport

Institute for Materials Research, National Bureau of Standards, Washington, D.C. 20234

(April 30, 1968)

The steady-state creep behavior of a dental amalgam subjected to tensile stresses of 500 to 4000 psi (3.4×10^6 to 2.8×10^7 N/m²) was investigated over the temperature range of 23 to 52 °C (296 to 325 K). It was found that the creep behavior can be represented by the equation:

$$\dot{\epsilon}_r = K\sigma^m e^{-E/RT}$$

where $\dot{\epsilon}_r$ is the creep rate, K and m are constants of the material, σ is the stress, E is the activation energy for the process, R is the gas constant and T is the temperature. Values of the constants determined for the dental amalgam were $K=2.31\times10^9$, $m=3.45$ and $E=35{,}300$ cal/mol (148,000 joule/mole).

Key Words: Amalgam; creep; creep activation energy; dental amalgam; silver amalgam.

1. Introduction

In a previous study of the viscoelastic behavior of dental amalgam [1][1] it was shown that the viscous strain rate of amalgam at a constant temperature is a nonlinear function of stress which can be represented by an equation of the form:

$$\dot{\epsilon}_r = K\sigma^m$$

where σ is the stress and K and m are constants of the material.

The objectives of the present study were (1) to determine the steady-state creep behavior of dental amalgam over a range of temperatures occuring in the mouth, (2) to determine which of the steady-state creep equations from established theory represents the behavior of dental amalgam, and (3) to determine the activation energy of creep of amalgam in order to gain an insight into the dominant mechanism governing the steady-state creep of amalgam.

2. Theory

The steady-state creep of a metal may be controlled by such processes as (1) true frictional forces, (2) thermally activated processes, and (3) quantum mechanical tunneling effects [2]. The quantum mechanical tunneling effects appear to occur only at very low temperatures, if at all. True frictional forces give rise to viscous or quasi-viscous behavior and in examples where quasi-viscous frictional forces appear to determine the creep rate, the energy is usually dissipated by a mechanism which is thermally activated. Thus, most steady-creep processes in metals are thermally activated processes; that is the creep rate depends on the temperature in the relation, $\exp(-E/kT)$ where T is the temperature and E is the activation energy of the specific process. The steady-state creep rate may be related to the thermally activated rate processes by the following general equation:

$$\dot{\epsilon}_r = \sum_i f_i(\sigma, T, \beta) e^{-E_i(\sigma, T, \beta)/kT} \qquad (2)$$

where

$\dot{\epsilon}_r$ = steady-state creep rate,
σ = applied stress,
T = temperature (kelvin),
β = a crystalline geometric factor,
E_i = activation energy for the process, and
k = Boltzmann constant (1.38×10^{-23} joule/kelvin).

The activation processes in a metal are controlled by such micromechanisms as (1) climb-softening

*This investigation is part of the dental research program conducted by the National Bureau of Standards, in cooperation with the Council on Dental Research of the American Dental Association; the Army Dental Corps; the Dental Sciences Division of the School of Aerospace Medicine, USAF; the National Institute of Dental Research, National Institutes of Health; and the Veterans Administration.

[1] Figures in brackets indicate the literature references at the end of this paper.

(climbing of dislocations) which is subgrain formation, (2) glide-softening (glide movement of dislocations) which is crystallographic slip, (3) flow of grain boundaries, (4) diffusion of vacancies (Nabarro-Herring mechanism) and (5) twinning [2].

Twinning occurs only at low temperatures and high stresses under tensile test conditions and therefore, is not ordinarily an important factor in steady-state creep [2].

The Nabarro-Herring mechanism contributes to steady-state creep only at temperatures near the melting point and at extremely low stresses [2].

The amount that flow of grain boundaries contributes to the steady-state creep is unclear, but it does contribute in some cases [2].

Glide-softening has as its main cause cross slip [3]. It can occur at low temperatures (below one half the melting temperature, T_m). Since glide-softening occurs while the dislocations are gliding, it occurs only at sufficiently high stresses and at short times in creep behavior and therefore, is not important in slow creep such as steady-state creep.

In the cases of climb-softening, the cause is vacancy creep [3]. Vacancy creep is a function only of temperature, not of stress. The mobility and concentration of vacancies must be great enough for vacancy creep to occur; this critical mobility and concentration of vacancies occurs for most metallic elements at approximately ½ the melting temperature of the element. Thus, climb-softening occurs for most metals only above 0.5 T_m and unlike glide-softening can occur at low stresses and allows large strains to develop over long periods of time. Therefore, climb-softening is one of the principle mechanisms of steady-state creep and is pronounced at temperatures above about 0.5 T_m. The climb-softening allows edge dislocations (1) to move out of their glide surfaces, (2) to annihilate or polygonize with other dislocations and (3) to pass around obstacles. The climb of the dislocations from their glide surfaces is achieved by absorbing or emitting vacancies. The forces necessary to achieve climb are obtained from local stress fields and the interaction with other dislocations; these forces are often small enough for creep due to climb-softening to be Newtonian [3] and described by the following equation:

$$\dot{\epsilon}_r = K\sigma e^{-E/RT}$$

where

$\dot{\epsilon}_r$ = steady-state creep rate,
σ = stress,
E = activation energy of self-diffusion,
R = gas constant, and
T = temperature (kelvin).

However, even though the steady-state creep may be controlled by Newtonian vacancy creep (climb-softening) the resulting creep may be non-Newtonian due to the fact that the number of climbing dislocations, their driving stresses and their climbing distances depend on the dislocation density which is dependent on the applied stress [3]. The rate of steady-state creep in the case of many metals may be represented by either of the following equations which are non-Newtonian in the stress relation but thermally activated:

$$\dot{\epsilon}_r = K\sigma^m e^{-E/RT} \text{ (Dorn equation)} \qquad [4, 5]$$

or

$$\dot{\epsilon}_r = Ae^{\beta\sigma} e^{-E/RT} \text{ (Kauzmann equation)} \qquad [6]$$

3. Experimental Procedure

The material and experimental procedures were as described by Oglesby, et al. [1]. Amalgam specimens were made by mixing mercury with a commercial alloy for dental amalgam (composition approximately Ag 70%, Sn 26%, Cu 3.5%, Zn 0.5%) and condensing the mixture into a metal mold. The dumbbell shaped specimens formed in the mold were 0.75 in (19mm) long, with a straight portion 0.3 in (8 mm) in length having a square cross section 0.1×0.1 in (2.5×2.5 mm).

Tensile stresses ranging from approximately 500 to 4000 psi (3.4×10^6 to 2.8×10^7 N/m^2) were applied to the specimens. Strain was measured to approximately 1×10^{-4} in per in with Tuckerman optical strain gages attached to the straight portion of the specimen. Creep rates were determined from the slope of the straight line portion of the loaded creep curve.

The steady-state creep rates were determined over the temperature range of 23 to 52 °C (296 to 325 K) and over the stress range of 500 to 4000 psi (3.4×10^6 to 2.8×10^7 N/m^2).

4. Results and Discussion

The steady-state creep rate was found to be nonlinear as a function of the stress for any fixed temperature, figure 1. It was further found that $\log_e$ of the creep rate was nonlinear as a function of stress at constant temperature. However, when the $\log_e$ of the creep rate was plotted as a function of the $\log_e$ of the stress a straight line was obtained at any given temperature, figure 2. These $\log_e \dot{\epsilon}_r$ versus $\log_e \sigma$ plots were made for fixed temperatures over the range 23 to 52 °C (296 to 325 K) and the slope of the straight line obtained at each temperature was determined and found to be approximately 3.5 for all the linear plots as shown in figure 2. This indicated that the steady-state creep rate could be approximated as a function of stress by the following relation:

$$\dot{\epsilon}_r = K\sigma^m f(T)$$

where m is the slope of the linear plot of $\log_e \dot{\epsilon}_r$ versus $\log_e \sigma$.

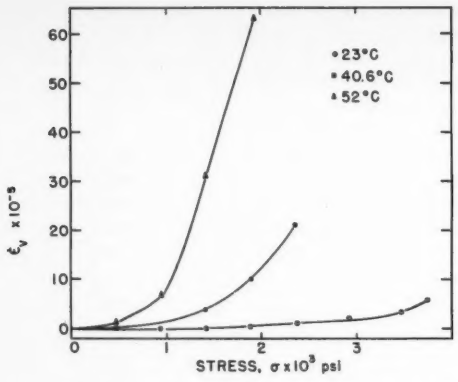

FIGURE 1. *Steady-state creep rate, ϵ_v, of dental amalgam versus stress.*

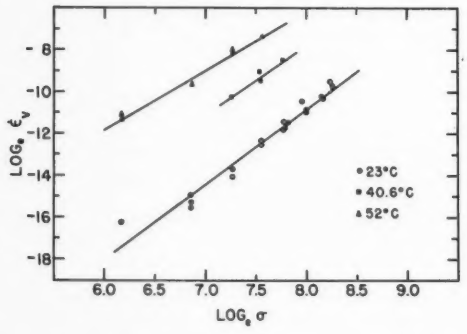

FIGURE 2. *Log$_e$ of steady-state creep rate, ϵ_v, of amalgam versus log$_e$ of stress, σ.*

Next the steady-state creep rate was examined as a function of temperature at various fixed stresses. The plots of creep rate versus T and $1/T$ were found to be nonlinear. However, a plot of the log$_e$ of the creep rate versus $1/T$ was found to be linear at fixed stress values of approximately 1400 and 1900 psi (9.6×10^6 and 1.3×10^7 N/m^2), figure 3; and straight lines were drawn through the two points for each of the other fixed stress values. The slope of these linear plots of log$_e$ $\dot{\epsilon}_v$ versus $1/T$ were approximately the same for the different fixed values of stress as shown in figure 3. Thus, the steady-creep rate $\dot{\epsilon}_v$ could be related to the absolute temperature by the following relationship:

$$\dot{\epsilon}_v = Ke^{-C/T}f(\sigma)$$

where C = the negative of the slope of the log$_e$ $\dot{\epsilon}_v$ versus $1/T$ where T is in kelvin. Now from theory [2] C is related to the activation energy of steady-state creep for a single micromechanism by the following relation:

$$E/R = C$$

where R is the ideal gas constant (1.99 calories per °C per mole; 8.31 joules per kelvin per mole). However,

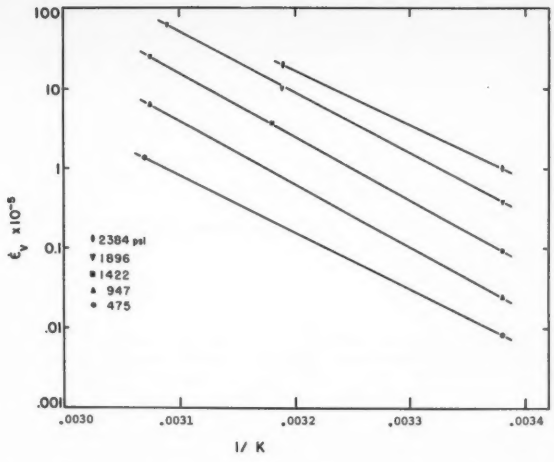

FIGURE 3. *Steady-state creep rate, ϵ_v, of amalgam plotted on a logarithmic scale versus the reciprocal of absolute temperature, K.*

when there are a number of micromechanisms involved the value of E is an average or combination activation energy usually representative of the dominant mechanism governing the steady-state creep process [2]. This activation energy E was calculated from the slopes in figure 3 and found to be about 35,000 cal/mole (150,000 joule/mole).

Combining the results obtained from the plots of log$_e$ of creep rate versus log$_e$ σ at a constant temperature and the plots of log$_e$ of creep rate versus $\frac{1}{T}$ at a constant stress gives the following equation for the steady-state creep of dental amalgam within the stress temperature ranges studied:

$$\dot{\epsilon}_v = K\sigma^m e^{-E/RT}.$$

A least squares fit of the equation

$$\log_e \dot{\epsilon}_v = \log_e K + m \log_e \sigma - \frac{E}{RT}$$

to all of the data gave the following values and standard deviations for the constants:

$m = 3.45 \pm 0.11$
$E = 35{,}300$ cal/mol $\pm$ 1,100 cal/mol (148,000 joule/mole $\pm$ 4,600 joule/mole)
$\log_e K = 21.6 \pm 1.5$.

In figure 4 a plot of log$_e$ $\dot{\epsilon}_v + \frac{E}{RT}$ versus log$_e$ σ shows a comparison of the experimental data with the curve calculated using these constants.

Since the steady-state creep rate of dental amalgam could be related to the temperature by the function exp $(-C/T)$, it is concluded that the dominant process controlling the creep rate of amalgam is a thermally activated one.

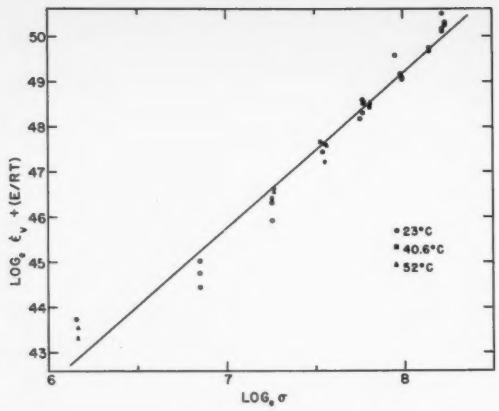

FIGURE 4. *Comparison of experimental points with curve calculated from the constants determined for the equation*

$$\dot{\epsilon}_v = K\sigma^m e^{-E/RT}$$

where
$\dot{\epsilon}_v$ = *steady-state creep rate*,
K = *2.31* × *10⁹*,
σ = *stress*,
m = *3.45*,
E = *35,300 cal/mol (148,000 J/mol)*,
R = *gas constant, and*
T = *absolute temperature (kelvin)*.

The results suggest that the dominant micromechanism involved in the creep of dental amalgam in the temperature range studied is diffusion controlled climbing of dislocations (subgrain formation). This is supported by the evidence that the controlling process is thermally activated and by the fact that the temperature involved is above 0.5 T_m. (The solidus temperature of amalgam as indicated by the appearance of liquid mercury is near 355 K.)

Activation energy for high temperature creep in pure metals corresponds generally to the activation energy of self diffusion [2, 3]. Little quantitative information is available on diffusion in dental amalgam. It is of interest to note, however, that the activation energy found for creep of amalgam lies within the range of energies of self diffusion reported for the metals, other than mercury, contained in dental amalgam, table 1.

TABLE 1. *Activation energy*

	Creep		Self-diffusion		Reference
	kcal/mol	*kJ/mol*	*kcal/mol*	*kJ/mol*	
Amalgam	35	146			
Silver			44–46	184–193	[7]
Tin	21–26	88–109	6–10	25–42	[7]
Copper	44	184	48	201	[2]
Zinc	27	113	20	84	[2]
Mercury	1.2	5.0	1.0–1.2	4.2–5.0	[8, 9]

Since the dominant mechanism controlling the thermally activated steady-state creep in amalgam in the range 298 to 328 K is probably climb of dislocations, the activation energy of which is the activation energy of diffusion, studies of the diffusion of the components into each phase of amalgam should be made to determine the activation energies. Also studies of the steady-state creep behavior of each phase of dental amalgam should be made to determine which phase or phases of dental amalgam dominate its steady-state creep behavior.

5. Conclusions

The steady-state creep behavior of dental amalgam in the temperature range 296 to 325 K and the stress range 500 to 4000 psi (3.4×10^6 to 2.8×10^7 N/m²) can be represented by the equation:

$$\dot{\epsilon}_v = K\sigma^m e^{-E/RT}$$

with $m = 3.45$ and $E = 35{,}000$ cal/mol (148,000 joule/mole).

The creep behavior is probably controlled by a thermally activated process dominated by the mechanism of climb of dislocations.

6. References

[1] Oglesby, P. L., Dickson, G., Davenport, R. M., Rodriquez, M. S., and Sweeney, W. T., Viscoelastic behavior of dental amalgam, J. Res. NBS **72C** (Engr. and Inst.), No. 3, 203 (1968).
[2] Schoeck, G., Theories of Creep, Chapter in Mechanical Behavior of Materials at Elevated Temperatures. Dorn, J. Ed. (McGraw-Hill Book Co., Inc., New York, 1961).
[3] Cottrell, A. H., The Mechanical Properties of Matter (John Wiley & Sons, Inc., New York, N.Y., 1964).
[4] Dorn, J. E., J. Mech. Phys. Solids **3,** 85 (1954).
[5] Weertman, J., Theory of Steady-State Creep Based on Dislocation Climb. J. Appl. Phys. **26,** 1213 (1955).
[6] Kauzmann, W., Flow of solid metals from the standpoint of chemical-rate theory, Trans. A.I.M.E. **143,** 57 (1941).
[7] Conrad, H., The Role of Grain Boundaries in Creep and Stress Rupture. Chapter in Mechanical Behavior of Materials at Elevated Temperatures, Dorn, J. Ed. (McGraw-Hill Book Co., Inc., New York, N.Y., 1961).
[8] Nachtrieb, M. H., and Petit, J., Self-diffusion in liquid mercury, J. Chem. Phys. **24,** 746 (1956).
[9] Hoffman, R. E., The self-diffusion of liquid mercury, J. Chem. Phys. **20,** 1567 (1952).

(Paper 72C3–279)

JOURNAL OF RESEARCH of the National Bureau of Standards—C. Engineering and Instrumentation
Vol. 72C, No. 3, July–September 1968

Publications of the National Bureau of Standards*

Selected Abstracts

A review of studies made on the decade fluctuations in the earth's rate of rotation, W. R. Davey, *Tech. Note 358 (Oct. 16, 1967) 20 cents.*

Studies of variations in the length of the day (l.o.d.) on the order of a few milliseconds over the period of a few decades are briefly reviewed. In this connection, studies of the dynamo theory of geomagnetism, the westward drift of the magnetic field, and electromagnetic core-mantle coupling preface the theory of the decade fluctuations in the l.o.d.

Key Words: Core-mantle coupling; decade fluctuations; dynamo theory; earth's core; geomagnetism; rotation of the earth; westward drift.

Activation analysis: Cockcroft-Walton generator, nuclear reactor, Linac, July 1966 through June 1967, Ed. J. R. DeVoe, *Tech. Note 428 (Nov. 1967), 55 cents.*

This is the first separate (not combined with that of Radiochemical Analysis) summary of progress for the Activation Analysis Section of the Analytical Chemistry Division of the National Bureau of Standards.

Pertinent information on the irradiation facilities of the nuclear reactor, Linac and Cockcroft-Walton generator are described. The initial installation of pneumatic transfer tubes is completed. Of great significance is the completion of a clean room that is used for pre-irradiation chemical separation for high sensitivity activation analysis.

A dual-sample biaxial rotating 14 MeV neutron-irradiation assembly has been tested. This assembly is part of a system that is controlled by a relay type of programmer to automate those irradiation steps that adversely affect precision of the analysis. This system was used to improve greatly the precision of analysis for oxygen and fluorine.

As a result of improved precision with the 14 MeV neutron irradiation, a study of systematic errors is now possible. Efforts to establish a reproducible correction factor for neutron and gamma-ray absorption between different matrices within the sample have shown considerable promise.

Standard Reference Material (SRM) steel chip Nos., 3b, 3c, and 30f have been analyzed for vanadium. Preliminary analyses of high purity platinum (a potential SRM) showed silver, copper, gold, palladium, and iridium at the ppm level. Future biological SRM's, (tree leaves, and beef liver) were tested for homogeneity and found satisfactory.

A variety of service analyses were performed. In particular, very pure aluminum was found to contain fractions of a ppm of chromium and scandium.

Additional efforts are being made to monitor reactor neutron fluxes. Additional nuclear instrumentation is being assembled to improve the versatility of the analysis technique.

Performance of the bremsstrahlung target, used with the linear electron accelerator, has been evaluated. Photon intensity distribution and stability was found to be within usable range. Analyses using the (γ, n) or (γ, p) reactions have been developed for magnesium in steels, and carbon in sodium metal.

Key Words: NBS reactor; NBS Linac; Cockcroft-Walton generator; digital computers; activation analysis; Standard Reference materials; photoneutron reactions; flux monitors; vanadium in irons and steels; homogeneity testing; biological, botanical samples; carbon in sodium; self absorption corrections; high precision 14 MeV neutron activation; instrumentation; flux monitors.

Activities of the NBS Spectrochemical Analysis Section, July 1966 through June 1967, Ed. B. F. Scribner, *Tech. Note 422 (Jan. 1968), 45 cents.*

A summary is given of activities of the NBS Spectrochemical Analysis Section for the year July 1966 through June 1967. In optical spectrometry, studies were made of (1) the effectiveness of a liquid Q-switch for laser pulse control and (2) the applicability of the high-frequency plasma torch in atomic emission and absorption spectroscopy. Two papers on laser probe spectrochemical analysis were published. In electron probe microanalysis an alignment procedure was developed for the x-ray spectrometer, data on x-ray mass absorption coefficients were collected and critically evaluated, and a review of techniques for scanning microprobe analysis was published. The factors entering into quantitative electron probe analysis are being investigated. In x-ray spectrometry studies were made of interferences especially in the analysis of complex alloys. A combination of techniques involving enrichment by electrodeposition, stable isotope dilution, and determination by the spark source mass spectrometer has provided an accurate method for trace analysis. Improvements in the Section's equipment, including digital readout devices, and developments in computer applications are also discussed. Listings are given of 15 publications and 23 talks by members of the Section during the year.

Key Words: Computing; digital readout; electron probe; gold analysis; isotope dilution method; laser probe; liquid Q-switch; mass attenuation coefficients; microphotometer; optical spectrometry; plasma torch; platinum analysis; preconcentration; selenium analysis; spark source mass spectrometry; spectrochemical analysis; standard reference materials; sulfur analysis; time-shared computer; x-ray absorption coefficients; x-ray fluorescence analysis; vacuum spectrometer.

Analytical coordination chemistry: titrimetry, gravimetry, flame photometry, spectrophotometry, and gas evolution, July 1966 to June 1967, Ed. O. Menis, *Tech. Note 424 (Jan. 1968), 55 cents.*

In the related areas of gravimetry, titrimetry, flame emission and atomic absorption spectroscopy, absorption and fluorescence spectrophotometry, and gases in metals, the versatile aspects of coordination chemistry have, in several instances, been uniquely exploited to yield either more precise and accurate results or lower detection limits. Fivefold improvement in the gravimetric analysis for beryllium has been obtained by means of an incomplete homogeneous precipitation followed by a selective spectrophotometric examination of the filtrate. In the field of thermal analysis a survey of fifteen compounds has revealed several promising, future standards for DTA studies covering the range of 75 to 900 °C. In the section on titrimetry highly precise procedures are described for the determination of boron and beryllium. Various instrumental parameters have been investigated in flame emission and atomic absorption spectroscopy in order to optimize such variables as nebulizer-burner and oxidant-fuel systems, elimination of interferences, and source difficulties. The use of chelate extraction systems has led to the extension of detection limits to the submicrogram level for impurities in zinc and selenium, while modified electronics

308-528 O - 68 - 3

has permitted the precise determination of 10 percent Li_2O in glass with a relative standard deviation of better than 0.2 percent. In absorption and fluorescence spectrophotometry the research aspect of ternary complexes or mixed chelates are described together with their potential use at the nanogram-picogram level. In the same area improvement in accuracy has been obtained by controlled dissolution of samples in closed systems with particular attention being given to the determination of arsenic in cast iron. Also described in this section is the differential spectrophotometric determination of dysprosium in a glass to be used as a neutron flux monitor, in which case the relative error was reduced to less than 0.25 percent. Finally, in the area of high vacuum fusion a new standard was certified for oxygen in titanium and in two titanium alloys. In addition, research in the use of the same technique for the determination of nitrogen has apparently eliminated the problem of low values that have in the past so frequently plagued the analyst.

Key Words: Absorption and fluorescence spectrophotometry; arsenic; atomic absorption; beryllium; DTA studies; dysprosium in a glass; flame emission; gases in metals; gravimetry; homogeneous precipitation; impurities in zinc and selenium; Li_2O in glass; nitrogen; oxygen in titanium; titrimetry.

Calculation of the properties of vacancies and interstitials. *Proceedings of a Conference May 1–5, 1966,* Ed. A. D. Franklin, *Misc. Publ. 287 (Nov. 17, 1967), $2.50.*
This is the Proceedings of a Conference on the Calculation of the Properties of Vacancies and Interstitials, Skyland, Virginia, USA, held on May 1–5, 1966. The Conference dealt with the theory and techniques of calculation of the properties of point defects in metallic and nonmetallic crystals. The contributed and invited papers divided about evenly among three major topics: (1) static-lattice calculations of the energies and configurations of simple vacancies and interstitials in, mainly, metals and ionic crystals; (2) electronic states at and near point defects in metals, rare gas solids, and insulators (*f*-centers, electron traps); and (3) vibrational states at point defects. The report of a panel discussion on each topic is also included. The emphasis is on the theory of the properties of isolated, simple defects rather than on the statistical properties of defect assemblies. The Conference attempted to examine the point defect theory and calculations critically, from the standpoint of general theory, rather than simply compare results with experiment.

Key Words: Calculations; electronic states; energies of formation; energies of motion; interstitials; point defects; theory; vacancies; vibrational states.

Disclosures on: Autosort—an automatic collating and sorting machine, optical heterodyne refractometer, liquid metering pump, stable wideband relaxation oscillator using three inverting amplifiers, and seat belt webbing abrasion resistance testing machine, Ed. D. Robbins and A. J. Englert, *Tech. Note 437 (Nov. 1967), 25 cents.*
This booklet presents descriptions and drawings of five devices that embody interesting and unusual solutions to problems frequently encountered in their respective fields. The devices are:

Autosort—An Automatic Collating and Sorting Machine
Optical Heterodyne Refractometer
Liquid Metering Pump
Stable Wideband Relaxation Oscillator Using Three Inverting Amplifiers
Seat Belt Webbing Abrasion Resistance Testing Machine

Key Words: Automatic document distribution; programmed document distribution; rotatable document bin array; optical refractive index; laser beam phase shift; laser heterodyning; flexible tubing pump; liquid metering pump; relaxation oscillator; inverting amplifiers; seat belt webbing abrasion; abrasion resistance testing.

Evaluation of information systems: A selected bibliography with informative abstracts, M. M. Henderson, *Tech. Note 297 (Dec. 1967), $1.00.*
A survey of the literature on evaluation of information systems has been conducted by the Technical Information Exchange, Center for Computer Sciences and Technology, National Bureau of Standards. During the early stages of the survey, the literature was divided among descriptions of programs which compared the performance of two or more information systems, accounts of programs which studied the performance of one system, papers and reports which discussed the problems of evaluation programs, and documents which proposed new techniques for evaluation of systems. From the total literature collected, those references which were judged to be most directly concerned with the subject of evaluation of information systems were selected and abstracted. The abstracts are designed to give a summary of the content of the corresponding paper; the author's own wording was used extensively, in order to avoid misinterpretation. All of the references collected are listed, in alphabetic order of authors' names, in the appendix to the main body of this publication.

Key Words: Evaluation; performance; testing of information systems; effectiveness; relevance.

Fire resistance of steel deck floor assemblies, H. Shoub and S. H. Ingberg, *Bldg. Sci. Series 11 (Dec. 1967), 25 cents.*
Tests were conducted to determine the resistance to fire of welded steel plate and beam floor assemblies with various conditions of floor covering on the plates, and ceiling protections beneath the beams. The trials included fire exposures from the burnout of combustible materials ranging from 10 to 40 lb/ft² on the floor surface as well as standard fire endurance tests in which the ceiling of the structure was exposed to fire.
The results of the tests indicated that the use of steel floor structures was practical from considerations of fire safety. For the test conditions established, fire exposure on top of the floor did not heat the structural steel supporting members sufficiently to cause load failure or collapse, and did not produce untenable conditions in the room below. In tests involving fire exposure to the underside of floors, the fire endurance times, based solely on heat transmission criteria, ranged from 1 hr 24 min to over 4 hr. Temperature levels attained by the structural members and deflection of the floor assemblies are also reported.

Key Words: Fire endurance; steel plate floors; burnout tests; floor tests; fire severity.

Low temperature mechanical properties of copper and selected copper alloys. A compilation from the literature, R. P. Reed and R. P. Mikesell, *Mono. 101 (Dec. 1, 1967), $2.75.*
In the past 60 years considerable data has accumulated concerning the mechanical properties of copper and its alloys. It was felt that there was a great need to adequately document these results in one publication. Therefore a unique type of compilation is presented. The compilation is divided into four parts. The first section is intended for quick reference use for those who are interested in average values. The second section includes data from most of the investigators who have published results on the mechanical properties of copper and its alloys. The third section is composed of tables classifying the investigations which were not included in section two. These usually involve investigations in which data were obtained only at one temperature, such as room temperature. The fourth section lists, in alphabetical order, all references used.

Key Words: Compilation; copper; copper alloys; low temperature; mechanical properties.

Radiochemical analysis: nuclear instrumentation, radiation techniques, nuclear chemistry radioisotope techniques July 1966 through June 1967, Ed. J. R. DeVoe, *Tech. Note 421 (Nov. 1967), 50 cents.*
This is the fourth summary of progress of the Radiochemical Analysis Section of the Analytical Chemistry Division at the National Bureau of Standards.
The section's effort comprises four major areas: Mössbauer spectroscopy, nuclear chemistry, nuclear instrumentation, and the application of statistics in nuclear and analytical chemistry.
A new design of transducer which is more compact than the previous design has been made so that low temperature experiments can be more easily performed. A method of simultaneously measuring two spectra with a single transducer has been devised. A single line nickel-61 source has been made and the magnetic moment of the excited 5/2 state has been measured with this source. Efforts have continued on the interpretation of the spectral parameters and their relation to structure analysis. Studies are continuing on the production of a standard for chemical shift of tin compounds.

Equipment is in the final state of assembly and initial testing for measuring cross sections of reactions such as (γ, ^{3}He) or (γ, ^{4}He) by mass spectrometry of the reaction products.
The precision of an analytical method must be carefully used when expressing a detection limit. In addition, care must be taken to be definitive about the meaning of a limit of detection. A suggested procedure for uniformity in reporting these often used terms is presented in this report.
The practical operation of Ge(Li) and Si(Li) detectors has been evaluated. It is found that careful control of the preamplifier noise and response is required for optimum performance.
A study of the precision and accuracy of gamma-ray excited x-ray fluorescence was made. Using as a basis the analysis of certified Standard Reference Materials, an improvement of a factor of two in precision was measured. The major advantage concluded from this work is that if rapid analysis requiring portability is desired, the radioisotopic source approach is useful.

Key Words: NBS Linac; computers; standard reference materials; photoneutron reaction; cross sections; flux monitors; nickel-61; Mössbauer spectroscopy; tin standard for chemical shift; PARLORS program for Mössbauer spectra; Mössbauer instrumentation; detection limits for analysis; solid state detectors.

Performance of square-edged orifices and orifice-target combinations as air mixers, T. K. Faison, Jr., J. C. Davis, and P. R. Achenbach, *Bldg. Sci. Series 12* (*Nov. 24, 1967*), *15 cents.*
A study was made at the National Bureau of Standards to determine the effectiveness of the square-edged orifice, or the orifice in combination with a target (circular baffle), for mixing an air stream which was initially nonuniform with respect to temperature. By achieving uniformity of temperature at all points within the cross section of an air stream, instrumentation for measurement might be simplified and a more representative temperature value obtained. Orifices having throat diameters of 8, 12, and 16 in were evaluated in a 24-in circular test duct to determine mixing effectiveness under selected test conditions of temperature distribution and flow rate. Targets of 8, 12, and 16 in in diameter in combination with a 12-in orifice were also investigated under similar conditions.
Graphic material is presented which illustrates how the orifice and orifice-target combinations perform as mixing devices under selected conditions. Results indicate that the 8-in (0.33 diam ratio) orifice effectively diminished the nonuniformity of temperature but only at a high pressure drop across the orifice and that a distance of 4.5 duct diameters was required for mixing.

Key Words: Diameter ratio; mixing effectiveness; square-edged orifice; temperature measurement; temperature pattern.

Selected tables of atomic spectra. Atomic energy levels and multiplet tables Si I, C. E. Moore, *NSRDS–NBS 3, Sect. 2*, (*Nov. 30, 1967*), *20 cents.*
The present publication is the second Section of a series being prepared in response to the increasing demand for a current revision of two sets of tables containing data on atomic spectra as derived from analyses of optical spectra.
Both the atomic energy levels and the multiplet table are included in the same publication, as parts A and B, respectively. The Sections are being prepared at irregular intervals for these spectra whose analyses are essentially complete. A flexible paging system permits the arrangement of the various Sections by atomic number regardless of the order in which the spectra are published in this series. Section 1 included three spectra of silicon, $Z = 14 \pm$ Si II, Si III, Si IV. The present Section contains similar data for Si I. The form of presentation is described in detail in the text to Section 1, and need not be repeated here.

Key Words: Atomic energy levels; atomic spectra Si I; multiplet table; silicon, first spectrum; spectrum, Si I; wavelengths, Si I.

Selected values of chemical thermodynamic properties, Tables for the first thirty-four elements in the standard order of arrangement, D. D. Wagman, W. H. Evans, V. B. Parker, I. Halow, S. M. Bailey, and R. H. Schumm, *Tech. Note 270–3* (*Jan. 1968*), *$1.25.* (*Supersedes Tech. Notes 270–1 and 270–2.*)
The tables contain values where known of the enthalpy and Gibbs energy of formation, enthalpy, entropy, and heat capacity at 298.15 °K (25 °C), and the enthalpy of formation at 0 °K, for all inorganic substances and organic molecules containing not more than two carbon atoms, for the first thirty-four elements in the Standard Order of Arrangement.

Key Words: Enthalpy of formation; entropy; Gibbs energy of formation; heat of formation; specific heat; thermodynamic properties.

Tables of bimolecular gas reactions, A. F. Trotman-Dickenson and G. S. Milne, *NSRDS–NBS–9* (*Oct. 27, 1967*), *$2.00.*
This survey covers the kinetics of bimolecular and termolecular gas reactions that do not involve atoms or molecules in electronically excited states. Bimolecular reactions are here defined as reactions in which two molecules are involved as reactants, that yield two or more molecules as products. Those reactions in which two molecules combine to form one molecule are most usefully considered as the reverse of unimolecular reactions which will be dealt with in another survey. Reactions of oxygen and nitrogen atoms have been omitted as they will also form the subject of another survey.
The literature from 1954 to December 31, 1965 has been exhaustively searched and it is hoped that for this period nothing has been omitted that should have been included.
The survey of earlier work has been based on one of the writers' books on "Gas Kinetics" which covered the literature to 1954. Use of the book for over ten years has revealed few omissions and these have been included in these tables. Data for the period January to August 1966 has been included where possible.

Key Words: Chemical kinetics; gas; bimolecular; reactions; reactions, tables; rate constants; activation energies; Arrhenius equation; data.

Tabulation of data on microwave tubes, J. K. Moffitt, *Handb. 104* (*Sept. 29, 1967*), *$1.25. Supersedes Handb. 70.*
A tabulation of microwave electron tubes with characteristics of each type has been arranged in the form of two major listings, a Numerical Listing in which the tubes are arranged by type number, and a Characteristic Listing in which the tubes are arranged by the kind of tube, and further ordered on the basis of minimum frequency and power output.

Key Words: Characteristics tabulation; microwave electron tubes; numerical.

Tabulation of data on receiving tubes, J. K. Moffitt, *Handb. 103* (*Sept. 29, 1967*), *$1.25. Supersedes Handb. 83.*
A tabulation of Receiving-Type Electron Tubes with some characteristics of each type has been prepared in the form of two major listings, a Numerical Listing in which the tubes are arranged by type number, and a Characteristic Listing in which the tubes are arranged by tube type and further ordered on the basis of one or two important parameters. The tabulation is accompanied by a listing of similar tube types and basing connections for the listed tubes.

Key Words: Basic connections; characteristics; electron tubes; numerical; receiving-type; similar types; tabulation.

High-precision coulometric iodimetry, G. Marinenko and J. K. Taylor, *Anal. Chem.* **39,** *No. 13, 1568–1571* (*Nov. 1967*).
On the basis of measurement of the potential of the working platinum anode as a function of current density and concentration of KI in solution, conditions were established for 100.0000% efficient generation of iodine. NBS Standard Reference Material arsenious oxide was analyzed utilizing optimum conditions for generation of iodine and for the stoichiometric reaction of arsenious acid with iodine. The precision of the method for titration of 0.5g samples of As_2O_3 is about 0.003%. Analysis of data for the assay of samples ranging in size from 100mg to 1g indicates no bias in the method. Coulometric assay of SRM 83c is $99.986 \pm 0.003\%$, which is in close agreement with the titrimetric comparison of 83c to iodine, purified by sublimation. This fact serves as additional evidence of the accuracy of the developed method.

Key Words: Constant-current coulometry; high-precision analysis; iodimetry; arsenious oxide; current efficiency.

Light scattering phenomena near the critical point, D. McIntyre and A. M. Wims (*Proc. 2nd Interdisciplinary Conf.*

Electromagnetic Scattering ICES–11, University of Massachusetts, Amherst, Mass., June 28–30, 1965), Book, Electromagnetic Scattering, Ed. R. L. Rowell and R. Stein, pp. 457–484 (Gordon and Breach, Inc., New York, N.Y., 1967).
The scattering from liquids and liquid mixtures near their critical points has been extensively studied in recent years. The existing experimental data are discussed with respect to their usefulness and limitations in sorting out the various statistical mechanical descriptions of critical phenomena. Scattering measurements on polystyrene-cyclohexane, cyclohexane-aniline, perfluoroheptane-isooctane, nitroethane-3-methylpentane are reported and discussed.

Key Words: Critical opalescence; light scattering; critical mixtures; binary mixtures; coexistence curves; phase separations.

Periodic acid, a novel oxidant of polycyclic aromatic hydrocarbons, A. J. Fatiadi, *Chem. Communications* **21,** *1087–1088 (1967).*
Certain polycyclic, aromatic hydrocarbons can be oxidized in good yield to quinones with paraperiodic acid in aprotic solvents containing a small proportion of water. No reaction was observed when oxidation was attempted with sodium periodate, instead of periodic acid. A possible reaction path for the oxidation has been suggested.

Key Words: Polycyclic aromatic hydrocarbons; paraperiodic acid; sodium periodate; aprotic solvent; reaction mechanism.

Machine oriented fingerprint classification system, J. H. Wegstein and J. F. Rafferty, *Proc. First Natol. Symp. Law Enforcement Science and Technology, March 7–9, 1967, Chicago, Illinois, Ed. S. A. Yefsky, 1, Chapt. V. Information Storage and Retrieval, 459–465 (Academic Press, Inc., New York, N.Y., 1967).*
The current state-of-the-art leads one to believe that computers and their associated high-speed mass stores can be utilized in handling large fingerprint files. Toward this end, a single-print classification system is explored. Requirements and objectives are listed. Needed measurements and statistical analyses of variations in details of fingerprints are identified.

Key Words: Fingerprint; automated classification system; ridge endings; bifurcations; minutia; descriptor; identification; Henry System.

Curve-fitting techniques and applications to thermodynamics, J. G. Hust and R. D. McCarty, *Cryogenics* **7,** *No. 4, 200–206 (Aug. 1967).*
The general problem of least squares fitting is considered. For completeness, derivations of well-known relations are included along with the developments of new techniques for imposing constraints on the unknown parameters, and of fitting data for several different properties simultaneously for both linear and non-linear equations. Several thermodynamic applications are included to illustrate the techniques developed.

Key Words: Curve fitting; least squares; thermodynamics; constraints; weighting; non-linear.

Application of computers to quantitative analysis of microstructures, G. A. Moore, Book, *Proc. Second Intern. Congress for Stereology, Chicago, Ill., Apr. 8–13, 1967, Ed. H. Elias, pp. 281–284 (Springer-Verlag, New York, N.Y., 1967).*
Stereological projections from any micrograph require evaluation of particle size and shape, thus observation on a dense raster limited only by the resolution of the microscope and observing system. The required large number of observations dictate automatic scanning and computer processing of the image. Results are limited by statistical inefficiency and precision of observation. Using high precision scanning equipment, the inaccuracies of measurement remain comparable to the limits imposed by statistics. Presently attainable precision is, however, an order of magnitude better than can normally be obtained by manual methods.
The presence or absence of a specific phase can be represented by a two-dimensional binary array which can be rapidly processed to yield the required measurements. Logical modification by the computer is frequently necessary to substitute for some of the logical discriminations normally made by the human analyst and to facilitate the desired measurements. Logical processes can reveal stereological relationships, construct morphological models, and dissect and describe the individual particles.

Key Words: Automatic scanning (of micrographs); computer processing (of micrographs); logical modification of pictures; precision scanning (of micrographs); quantitative microscopy; stereological analysis.

The metric system in Illuminating Engineering, L. E. Barbrow, *Illum. Engr.* **LXII,** *No. 11, 638–640 (Nov. 1967).*
The most commonly used unit of illumination in the USA is the footcandle. There are two commonly used units of luminance, the footlambert and the candela per square inch. The growing international adoption of SI units makes it advisable for illuminating engineers to introduce the use of these units in their publications in the immediate future and to understand the implications of the use of the SI units. The SI unit of illumination is the lux (one lumen per square meter). The SI unit of luminance is one candela per square meter (sometimes named the nit). One of the basic principles and advantages of SI is that there can be only one unit for each quantity; thus there cannot be an SI unit similar to footlambert which is expressed in terms of lumens per unit area. Council of the Illuminating Engineering Society has been officially requested to (1) approve the policy of having SI units given primary use in its publications, and (2) promote the depreciation of "lumens per unit area" as a unit of luminance and sponsor its use solely as a unit of luminous exitance (formerly emittance).

Key Words: Exitance; illumination; luminance; lux; metric units; nit; SI units in illuminating engineering.

Contribution of thermal noise to the line-width of Josephson radiation from superconducting point contacts, A. H. Silver, J. E. Zimmerman, and R. A. Kamper, *Appl. Phys. Letters* **11,** *No. 6, 209–211 (Sept. 15, 1967).*
The line-width of the radio-frequency Josephson oscillation of a voltage-biased superconducting point contact has been measured between 1.3 and 4.2 °K, with bias resistors between 1.7×10^{-10} and 2.6×10^{-5} ohms. Within the experimental accuracy, the line-width is proportional to RT, the constant of proportionality being of the order of k/φ_0^2 (Boltzmann's constant divided by the square of the flux quantum).

Key Words: Thermal noise; Josephson radiation; line-width; superconductivity; point contacts.

Electron diffraction studies of active, passive, and transpassive oxide films formed on iron, C. L. Foley, J. Kruger, and C. J. Bechtoldt, *J. Electrochem. Soc.* **114,** *No. 10, 994–1001 (Oct. 1967).*
Iron foil specimens were anodically polarized by means of a potentiostat in 1N H_2SO_4, 0.1N NaOH and a sodium borate boric acid solution (pH, 8.5). Both passive, active and transpassive regions of the polarization curve were studied for each solution. The oxide films were examined while still in contact with the iron foil by selected area transmission electron diffraction. Five iron planes were studied: {100}, {110}, {111}, {210} and {211}, and the epitaxial relationship of the oxide to the iron substrate determined. Evidence was found indicating that in all of the electrolytes used the passive film contained γ-Fe_2O_3, while the non-passive films did not.

Key Words: Electron diffraction; gamma-Fe_2O_3; iron; passivation.

Negative dispersion and brillouin scattering, R. D. Mountain and T. A. Litovitz, *J. Acoust. Soc. Am.* **42,** *No. 2, 516–517 (Aug. 1967).*
The fluctuations in density observed in Brillouin scattering may be represented as temporally absorbed waves. Negative dispersion occurs for these waves although it may be masked by positive dispersion due to relaxation processes. Numerical estimates of velocity and of negative dispersion are made for CCl_4 at 20 °C. The importance of measuring both the position and the width of the Brillouin peaks in order to obtain the elastic modulus of the liquid is stressed.

Key Words: Brillouin scattering; elastic modulus; liquid; negative dispersion relaxation of viscosity; temporal absorption.

Response of pneumatic pressure-measurement systems to a step input in the free molecule, transition, and continuum flow regimes, *J. Hord, ISA Trans.* **6,** *No. 3, 252–260 (July 1967).*
A simplified analysis of the response of pressure-sensing devices and their interconnecting tubing is presented. The results are

conveniently presented in the form of time equations, with the fractional change in the applied step (usually 63.2%) as the variable. A single algebraic equation adequately predicts (within about ±20%) the response of simple pressure-measuring systems in the free molecule, transition and continuum flow regimes. Two very simple algebraic equations (for free molecule and continuum flow) may be used to predict time response throughout the flow regimes if a maximum error of about 2:1 (predicted time constants are 2 times too large) is tolerated in the mid-transition range. The criterion is given for extension of these formulae into the transition flow range. The formulae are limited to relatively small pressure steps in the viscous flow region (Poiseuille flow) and are not restricted for free molecule flow. All of the formulae developed are suitable for field engineering applications. The existing literature is synthesized by comparison with the analysis. The relative importance of the numerous variables encountered in this type of analysis is discussed.

Key Words: Response of pneumatic pressure-measurement systems in the free molecule, transition, and continuum flow regimes; response of pneumatic pressure-sensing tubulation; response of pneumatic transmission lines; time constants of pneumatic pressure lines; time lag and delay in pneumatic pressure-sensing lines; time respons of pneumatic pressure-sensing systems to step inputs.

Diminishing discoloration in methacrylate accelerator systems, R. L. Bowen and H. Argentar, *J. Am. Dental Assoc.* **75,** *No. 4, 918–923 (Oct. 1967).*
A method was devised for accentuating the formation of discoloration products that may form during the free radical polymerization of methacrylates at room temperature. Various accelerators and stabilizers were compared on an equimolar basis. The selection of the materials was based on literature information regarding current theories of free radical polymerization and the absorption of visible light by organic compounds. The use of the sterically hindered phenol, butylated hydroxytoluene, did not produce discoloration whereas, the use of hydroquinone or the monomethylether of hydroquinone had a darkening effect. A compound (N,N-dimethyl-3, 5-dimethylaniline) was synthesized which was an effective accelerator and which produced less discoloration than did N,N-dimethyl-p-toluidene.

Key Words: Color formation; discoloration; methacrylate; polymerization; N,N-dimethyl-3, 5-dimethylaniline; accelerators.

Metallo-organic polymers, E. Horowitz, *Mod. Plastics* **45,** *No. 3, 146–148 (Nov. 1967).*
Certain organic molecules containing electron-donating groups such as derivatives of bis(β-hydroxyquinoline) can be reacted with metal ions to yield metallo-organic polymers in which the metal atoms are linked in the backbone. Both linear and cross-linked polymers have been prepared and their thermal stabilities have been investigated. It has been shown that the thermal stability of these polymers is related to the properties of the metal and the composition of the organic component.

Key Words: Metallo-organic polymers; synthesis; thermal stability; role of metal and ligand.

Thermal titration of platinum black and the initial heat of adsorption for hydrogen, E. S. J. Tomezsko and G. T. Furukawa, *J. Catalysis* **8,** *No. 4, 386–388 (Aug. 1967).*
The heat of adsorption of hydrogen on platinum black was investigated by means of an automatically controlled adiabatic calorimeter. When the platinum black was carefully freed of adsorbed oxygen, no rapid decrease was observed in the heats of adsorption with increasing coverage of hydrogen. The heat of adsorption of hydrogen on clean platinum surface was found to be 17.5 (73.2 kv/mole) kcal/mole of hydrogen, with an estimated uncertainty of ±0.2 kcal/mole (±0.8 kv/mole).

Key Words: Adsorption of hydrogen on platinum black; heat of adsorption of hydrogen; platinum black; thermal titration.

Volume changes accompanying collagen denaturation, R. G. Christensen and J. M. Cassel, *Biopolymers* **5,** *685–689 (1967).*
A dilatometric technique is employed to measure the volume changes occurring on denaturation of collagen solutions and tendons. Partial specific volumes of tropocollagen are calculated to be 0.686 ml/g in water and 0.689 ml/g in 0.1M citrate buffer. From data on nonaqueous solutions, it is estimated that most of the volume change arises from changes in polymer configuration rather than from changes in solvation.

Key Words: Partial specific volume; collagen; dilatometry; denaturation; solvation; hydration.

Development of a method for testing and rating refrigerated truck bodies, C. W. Phillips and R. W. Penny, *USDA Tech. Bull. No. 1376 (Superintendent of Documents, Government Printing Office, Washington, D.C. 20402, Sept. 1967, 15 cents).*
A recommended standard method is presented for testing and rating the cooling load due to heat transmission and air and moisture leakage into refrigerated truck bodies used for stop and go delivery of perishable chilled or frozen food. Results of laboratory tests of five typical vehicles, with and without simulated solar heating, were used as a basis for determining criteria for the testing and rating procedure. A steady-state test procedure, with appropriate multipliers to account for solar heating is recommended. Rating conditions of 0 °F and 35 °F interior temperature and 100 °F and 50 percent ambient temperature and relative humidity are suggested. Means for calculating air leakage rate from observed weight gain rate under standard test conditions are incorporated. Measurement of service cooling loads caused by warm cargo or by air exchange through opening and closing of doors is not included in the recommended procedure. However, such service loads must be considered in determining the capacity of an adequate refrigeration system.

Key Words: Rating and testing; cooling loads; refrigerated truck bodies; simulated solar heating; weight gain; air leakage.

Experimental apparatus and procedures for evaluating parameters affecting the pumping efficiency of a cryogenically cooled plane, L. O. Mullen and M. J. Hiza, *J. Vacuum Sci. Technol.* **4,** *No. 5, 219–229 (Sept.–Oct. 1967).*
The collection efficiency of a plane acting as a pump in a vacuum system can be determined by measuring the rate at which molecules of a given species strike and the rate at which they return from that plane. This paper discusses an experimental vacuum system incorporating a moveable partial pressure analyzer capable of making such measurements. The experimental procedure discussed here provides a means for evaluating parameters affecting the pumping efficiency. Efficiency values obtained by the present approach are compared with values obtained from kinetic theory and from speed factor measurements. The experimental data show that much of the deviation of reported pumping efficiencies can be explained by fragmentation of the test gas molecules and by a pressure anisotropy in the test dome. A means of calibrating the analyzer with vapor pressure data is also discussed.

Key Words: Capture coefficient; cryocondensation; cryogenically cooled surfaces; cryopump; partial pressure measurements; pressure calibration with vapor pressures; pressure anisotropy; pumping efficiency; pumping speed; speed factor measurements; sticking coefficient; vacuum techniques.

Improving pressure and vacuum measurement standards, E. C. Lloyd, *Instr. Control Systems* **40,** *No. 9, 105–109 (Sept. 1967).*
Results of the NBS developments are outlined in a number of projects relating to standards for improved measurement of pressures throughout the range from vacuum to very-high pressures. In the vacuum range this includes techniques for generation of stable reference pressures, and improved absolute instruments for force per unit area measurement down to 10^{-9} torr. In the range from a few millibars to hundreds of kilobars the use of fixed points, and the performance of improved piston gages and interpolation instruments, are described. Problems presently limiting accuracy of calibration and NBS investigations of possible solutions are mentioned. Two new "accuracy charts" are presented showing present and possible future NBS capabilities.

Key Words: standards; calibration; measurement, pressure; vacuum; accuracy.

Configuration of isolated polymer molecules adsorbed on solid surfaces studied by Monte-Carlo computer simulation,

F. L. McCrackin, *J. Chem. Phys.* **47,** *No. 6, 1980–1986 (Sept. 15, 1967).*
The configurations of adsorbed polymer molecules with excluded volume were simulated on a four-choice simple cubic lattice using a computer. The average values of the fraction of segments on the surface, loops off the surface, normal distance of the end of the molecule from the surface, root-mean-square of the normal distance, maximum normal distance from the surface, and root-mean-square end-to-end distance were calculated for various lengths of the molecules and attractive energies to the surface. When these averages over the configurations are compared with previous results which had neglected the excluded volume effect and important differences are found.

Key Words: Adsorption; configurations; four-choice cubic lattice; Monte Carlo; polymers.

Ears on the line profile of decay transitions in a gas laser, W. G. Schweitzer, Jr., M. M. Birky, and J. A. White, *J. Opt. Soc. Am.* **57,** *No. 10, 1226–1230 (Oct. 1967).*
In a gas laser a spectrum line whose upper state is the lower state of the laser transition may contain a structure due to the laser action. We have observed this structure, which we refer to as *ears*, on the 6096Å Neon line emitted spontaneously in a 1.15 μm He-Ne laser. The width of the *ear* was measured interferometrically and compared with the width predicted from the phenomenological width γ_{ab}/π in the laser transition.

Key Words: Laser; line profile; lifetime; neon.

Nuclear magnetic resonance in sodium thallide, L. H. Bennett, *Acta. Met.* **14,** *No. 8, 997–999 (1966).*
The nuclear magnetic resonance signal for $Ti^{203, 205}$ is observed in sodium thallide alloys. It is determined that the previously reported negative Knight shift value of one percent for NaTl was essentially correct, and the more recently reported negative value of one-half percent was in fact for $NaTl_2$. A crystal structure is proposed for $NaTl_2$.

Key Words: Nuclear mangatic resonance; sodium; thallium; alloys; intermetallic; compounds; x-ray diffraction; Knight shift.

Nuclear Magnetic resonance in zintl intermediate phases LiCd and LiZn, L. H. Bennett, *Phys. Rev.* **150,** *No. 2, 418–420 (Oct. 1966).*
The nuclear magnetic resonances have been observed for Li^7 and Cd^{113} in LiCd and for Li^7 and Zn^{67} in LiZn. The Knight shift for $LiCd^{113}$ is 0.39% for $LiZn^{67}$ 0.20%, for LiCd or LiZn less than 0.01%. An energy band scheme is proposed.

Key Words: Zintl phase; LiCd; LiZn; β-32 structure; nuclear magnetic resonance; Knight shifts, linewidths.

Nuclear quadrupole resonance thermometry, D. B. Utton, *Metrologia* **3,** *No. 4, 98–105 (Oct. 1967).*
The nuclear quadrupole resonance frequency of ^{35}Cl in $KClO_3$ has been studied in the temperature range 12 °K–297 °K. The combined uncertainties in the frequency and temperature measurements correspond to ± .001 °K in the range 50 °K–297 °K, deteriorating to ± .004 °K at 30 °K and ± .010 °K at 20 °K. Both the nuclear resonance spectrometer and the temperature control apparatus are described. The experimental data are fitted to a theoretical expression in the temperature range 12 °K–90 °K; at higher temperatures the data are fitted to empirical polynomials.

Key Words: Nuclear quadrupole resonance thermometry 12 °K–297 °K; potassium chlorate; instrumentation.

Sapphire window mountings for low temperature spectroscopy, L. J. Schoen, *Rev. Sci. Instr.* **38,** *No. 10, 1531–1532 (Oct. 1967).*
Two newly designed sapphire window mountings suitable for use at cryogenic temperatures are described. These should prove valuable in maintaining efficient, reproducible and trouble free thermal contact with conventional refrigerants.

Key Words: Cryostat; deposit; thermal contact; thermal conductivity; window holder.

Stochastic theory of multistate relaxation processes, I. Oppenheim, K. E. Shuler, and G. H. Weiss, *Adv. Mol. Relaxation Processes* **1,** *No. 1, 13–68 (Nov. 1967).*
The stochastic theory of multistate relaxation processes is discussed with special reference to Markov Processes, the derivation and properties of the Master Equation, the derivation and properties of the Fokker-Planck Equation and First Passage Time problems. The theory developed is then applied to a number of examples.

Key Words: Stochastic processes; relaxation processes; markov processes; Fokker-Planck equation; master equation; first passage times.

Transitions in vapor-deposited alumina from 300 to 1200 °C, A. L. Dragoo and J. J. Diamond, *J. Am. Ceramic Soc.* **50,** *No. 11, 568–574 (Nov. 1967).*
The transition of amorphous alumina to α-alumina was studied by x-ray diffraction, electron diffraction, DTA, TGA, and microscopic observation. The amorphous alumina was prepared by evaporation of molten alumina *in vacuo* and its deposition on the glass envelope of the vacuum chamber. Two transition paths were observed after the amorphous alumina passed through an initial crystallization region (between 570 and 670 °C at 16 hours). The principle sequence was γ-, to δ- to α-alumina. A minor amount of θ-alumina developed from the initial crystallization and persisted throughout the duration of the former sequence as a parallel path. Some conversion of δ- to θ-alumina was detected above 900 °C. DTA produced an unexplained exothermic peak at 320° and a second exothermic peak at 860° which corresponded to formation of metastable aluminas.

Key Words: Alumina, alpha alumina, amorphous alumina, delta alumina, gamma alumina, intermediate aluminas, metastable aluminas, phase transitions, theta alumina

Lunar tides in the ionosphere, S. Matsushita, *Encyclopedia of Physics XLIX/2, 547–602 (Springer-Verlag, Berlin, Germany, 1967).*
All previous work on lunar tidal variations in the ionospheric F2, F1, E, Es, and D layers by various researchers are thoroughly reviewed and are compared with recent results of lunar tides obtained from ionospheric electron density profile data and also with radio observations of lunar tidal winds in the ionosphere. A world-wide behavior of the lunar tides in different ionospheric layers is then obtained. After reviewing lunar tidal variations in the surface atmosphere, geomagnetic lunar variations at several places are examined, and a new lunar current system at about 100 Km altitude is suggested. Based on this current system the lunar tides in the ionosphere are discussed theoretically, taking into consideration both hydro and electro dynamical motions.

Key Words: Ionosphere; lunar tides; lunar variations; surface atmospheres.

Analysis of gold and platinum group alloys by x-ray emission with corrections for interelement effects, J. D. Eick, H. J. Caul, D. L. Smith, and S. D. Rasberry, *Appl. Spectry.* **21,** *No. 5, 324–328 (Sept.–Oct. 1967).*
The x-ray emission analysis of noble metal alloys was investigated critically to determine optimum conditions for accurate analysis. The analytical curves for the elements Cu, Pd, Pt, and Zn were found to be linear with a deviation of less than ±0.2 percent. However, a nonlinear relationship existed for gold and for silver. These discrepancies could not be eliminated by variation in sample preparation. An interelement effect due to x-ray absorption and enhancement was found and was corrected to an accuracy of 0.2 percent by means of a mathematical treatment suggested by Lucas-Tooth and Price. The analysis by x-ray emission can be accomplished in approximately one-tenth of the time necessary for conventional wet chemical methods.

Key Words: Gold and platinum group alloys; noble metal alloys; x-ray emission.

Chemical changes induced by high energy radiation. The present state of our knowledge, P. Ausloos, *Scientia CII, 1–14 (Sept.–Oct. 1967).*
The chemical changes in matter brought about by absorption of low energy radiation such as visible and ultraviolet light have been intensively investigated for several decades. On the other hand, the

chemical transformations induced by high energy radiation (X, gamma, β, α-rays) were long considered to be of such complexity that the task of unravelling them was considered insurmountably difficult. However, during the last decade, impressive advances have been made towards achieving an understanding of the fundamental chemical processes induced by high energy radiation. Many experimental techniques, some of which are new and some of which have been used in other areas of physics or physical chemistry, have now been brought to bear on the problem. Through these various approaches definitive information has been obtained concerning the existence and reactions of the various highly reactive intermediate species (radicals, ions, excited molecules produced by high energy radiation). The understanding of such systems has now reached a degree of sophistication such that high energy radiation can be used to obtain accurate information about various well defined chemical and physical processes which are of general scientific interest.

Key Words: High-energy radiation; chemical changes; ion-molecule reactions; free radical reactions.

Criteria for selection of absorber mounting materials in Mössbauer spectroscopy, L. May and D. K. Snediker, *Nucl. Instr. Methods* **55,** *183–188 (1967).*
The criteria for the selection of materials for mounting absorbers include their mechanical and chemical properties and their attenuation of the γ-rays and X-rays emitted from the Mössbauer source. Attention of the 14.4-keV γ-ray and 6.3-keV X-ray associated with ^{57}Fe was measured for nine commercial materials including plastics and metals. The linear absorption coefficients and half-thicknesses for each material were measured. The usefulness and limitations of each material are discussed, along with three different absorber mounting techniques.

Key Words: Absorber mounting devices; absorption coefficients; gamma-rays and x-rays; half-thickness; Mössbauer spectroscopy; 14.4-keV.

Determination of medium-weight elements by gamma-excited x-ray fluorescence, M. C. Hollstein and J. R. DeVoe, *(Proc. Second Symp. on Low Energy X- and Gamma Sources and Applications, University of Texas, Austin, Texas, Mar. 27–29, 1967), ORNL–IIC–10, pp. 483–502 (1967).*
The application of gamma-excited x-ray fluorescence in the determination of medium weight elements has been studied. The pertinent components of the spectrometer are an ^{241}Am source and a solid state detector, with a low-noise preamplifier and multi-channel analyzer. The resolution of the system is between 1.2 and 1.3 keV (FWHM) for 8 to 45 keV photons. Three different techniques of sample mounting were investigated. For single elements in the range from Cu to Dy the estimated detection limits are 10–100 μg and 0.01–1 mg/ml, depending upon the sample mounting procedure. The corresponding K_α-peak intensities are $2\times10^4-3\times10^3$ cpm per mg and $4\times10^4-6\times10^2$ cpm per mg/ml, respectively. For testing the application of the method two series of NBS Standard Reference Materials were analyzed for Sn and Mo as minor constituents within a concentration range from about 0.04 to 9%. The best results were obtained by direct counting of the solid samples. Using this technique, a non-destructive analysis for Mo and Sn can be performed in a relatively short time with a precision of a few percent, a detection limit of about 100 ppm and a sensitivity of 6×10^3 to 1.4×10^4 cpm per percent concentration.

Key Words: Quantitative analysis; tin; molybdenum; medium weight elements; X-ray fluorescence; gamma-excitation.

Evaluation procedures and annual performance data for Leclanché cells, W. J. Hamer, *Electrochem. Technol.* **5,** *No. 11–12, 490–498 (Nov.–Dec. 1967).*
This paper deals with the development over the past 48 years of so-called "standardized tests" for the evaluation of Leclanché cells and batteries. Data covering this time period or a part of this time period are given for (1) general-purpose flashlight cells, (2) industrial flashlight cells, (3) railroad lantern batteries, (4) photoflash cells, (5) No. 6 cells for various end uses, (6) radio "A" batteries, (7) radio "B" batteries, (8) hearing-aid "A" batteries, (9) hearing-aid "B" batteries, and (10) transistor hearing-aid batteries. The presently used standard tests, 27 in number, are described. A history of the development of dry cells of the Leclanché type is also included.

Key Words: Dry cell tests, dry cell standards; battery nomenclature; advances in dry cells; dry cell specifications; international dry cell standards.

Glass-membrane potentials in mixed anion melts, K. H. Stern, *J. Electrochem. Soc.* **114,** *No. 12, 1257–1258 (Dec. 1967).*
The emf of the four-ion concentration cell with membrane

$$Ag|Ag^+, Na^+, Cl^-, Br^-|glass|Ag^+, Na^+, Cl^-, Br^-|Ag$$

is derived for the case $X_{Na^+} \ll X_{Ag^+}$ by assuming that the cationic chemical potentials are additive functions in the mole fractions of the thermodynamic components, e.g., $\mu_{Ag^+} = X_{AgCl}\mu_{AgCl} + X_{AgBr}\mu_{AgBr}$. For solutions very dilute in sodium, corrections for non-ideality are negligible. Experimental results agree satisfactorily with calculated ones.

Key Words: Molten salts; galvanic cells; membrane potentials.

Multiplex for dual-spectrum Mössbauer spectrometry, F. C. Ruegg, *(Proc. Second Symp. on Low Energy X- and Gamma Sources and Applications, University of Texas, Austin, Texas, Mar. 27–29, 1967), ONRN–IIC–10, pp. 157–175 (1967).*
It is often desirable to have the capability of accumulating two Mössbauer spectra simultaneously with both spectra having exactly the same Doppler velocity dependence. This is possible with a multiplexing system which allows accumulation of two spectra simultaneously and storing of each spectrum in a 200 channel subgroup of a multichannel analyzer. The memory of the analyzer which is operated in the time mode is used on a demand basis by the two detector systems, and the counts are routed to the proper subgroup in complimentary channel locations, i.e., the channel location in the second subgroup is the channel number in the first subgroup plus 200. The logic, circuitry and performance are described.

Key Words: Multiplex; Mössbauer; dual spectra; spectroscopy.

New developments in zinc oxide-eugenol cement, G. M. Brauer, *Ann. Dentistry* **26,** *No. 2, 44–50 (1967).*
During the last few years considerable interest has been generated in improving zinc oxide-eugenol materials. A better understanding of the setting mechanism of these cements has become available which has lead to the development of modified ZOE cements usually containing *o*-ethoxy-benzoic acid (EBA). These materials show reactions to the tissues including the dental pulp similar to ZOE cements. Physical properties of the EBA containing cements approach those of the biologically less desirable zinc phosphate cements.

Key Words: EBA cements; zinc oxide eugenol cements; dental materials; dental cements; new developments in dental materials.

Pertinent data on some physical properties of different investments used in the casting of gold alloys, M. Ohashi, J. W. Stanford, and G. C. Paffenbarger, *J. Nihon Univ. Sch. Dent.* **9,** *No. 3, 121–126 (Sept. 1967).*
Fineness, time of setting, compressive strength, linear thermal expansion, hygroscopic expansion, normal setting expansion, and surface defects of alloy castings were determined using casting investments of three types thermal inlay, hygroscopic inlay, and thermal partial denture. The use of the normal setting expansion combined with either the hygroscopic or thermal expansion to compensate for the shrinkage of casting gold alloys is discussed.

Key Words: Alloy castings; gold alloys; hygroscopic inlay; thermal inlay; thermal partial denture.

Qualitative and quantitative determination of emulsion-polymerised binders in latex paints, M. A. Post, *J. Appl. Chem.* **17,** *315–320 (Nov. 1967).*
Methods for the separation and identification by infrared absorption spectroscopy of styrene-butadiene, acrylic, vinyl-acrylic and polyvinyl acetate homopolymer and dibutyl maleate copolymer in emulsion paints based on these materials are presented. Detailed procedures for their quantitative determination are discussed.

Key Words: Acrylic; identification; infrared spectroscopy; latex paints; polyvinyl acetate; separation; styrene-butadiene; vinyl-acrylic.

A flattery index for artificial illuminants, D. B. Judd, *Illum. Eng.* **62,** *No. 10, 593–598 (Oct. 1967).*
Artificial illuminants are used for (1) light-dark discrimination of objects, (2) critical appraisal of colored objects, and (3) appreciative viewing of colored objects. A light source that renders object colors in accord with their preferred colors may be said to flatter those objects. A flattery index has been derived for light sources used for appreciative viewing of colored objects to measure the degree to which such sources render object colors as we would like to see them. This index is based solely on spectral distribution and is modeled after the index of color rendition recently recommended by the CIE. It uses 10 of the 14 test samples established for appraisal of color rendition, and it uses the same definition of reference illuminants. It is scaled so that the reference illuminant receives a flattery index of 90, and a test illuminant rendering object colors precisely in accord with the preferred colors of the test samples receives a flattery index of 100. The test sample representative of the human complexion receives about one-third of the total weight; the two test samples representative of food colors, about one-third; the seven other test samples, the remainder.

Key Words: Color; flattery; illuminants; preference; rendition of color.

An analysis of the "quarter-wave" technique of reducing the errors in UHF and microwave impedance measurement, W. E. Little, D. A. Ellerbruch, and G. F. Engen, *IEEE Trans. Microwave Theory Tech.* **MTT-15,** *No. 9, 504–507 (Sept. 1967).*
An analysis is given of the "quarter-wave" impedance measurement technique. This technique, which finds its widest potential application in conjunction with standing wave machines, permits the approximate elimination of the error due to residual reflection or VSWR. If the other sources of error are small, the potential reduction in error is in the ratio $|t_{11}|/2|S_{11}|$, where S_{11} and t_{11} are the residual reflection coefficients of the standing wave machine and quarter wavelength section respectively.

Key Words: Impedance measurement; reflection coefficient measurement; quarter wave; standing wave machine; UHF; microwave.

Accelerometer resonances affect vibration measurement, E. T. Pierce, O. W. Price, S. E. Edelman, and E. Jones, *J. Environ. Sci.* **10,** *No. 6, 17–21 (Dec. 1967).*
Errors in vibration measurement can be caused by unintended relative motion in the pickup. Near the resonant frequency of such relative motion, the pickup can affect the motion of surface to which it is attached. The paper gives details of two cases of resonances of this kind: resonances which are unexpected on the basis of the usual mass-spring theory.

Key Words: Accelerometer; resonance; vibration; pickup; calibration.

Preparation of electron probe microanalyzer standards using a rapid quench method, J. I. Goldstein, F. J. Majeske, and H. Yakowitz, *Advan. X-ray Anal.* **10,** *431–446 (1967).*
Standards for microprobe analysis can be made to serve two purposes: (1) Proposed correction models can be tested with them and (2) Analysis can be performed more accurately in the system which includes the standard. Few microprobe standards are presently available because they must be homogeneous on the micron scale and their composition must be known accurately. A modified Duwez splat cooling method is described which enables the investigator to prepare suitable standards in most cases. The apparatus which is relatively simple and inexpensive is described in detail. The systems Au-Si and Al-Mg were chosen as test cases. Suitable standards were prepared at different concentrations in each system. The analytical results for all compositions in Al-Mg are presented and discussed.

Key Words: Al-Mg; Au-Si; electron probe standards; quantitative microanalysis; standard preparation; splat cooling.

The National Bureau of Standards program in computer sciences and technology, H. R. J. Grösch, *Stat. Reptr. 68–3, 37–41 (Superintendent of Documents, Government Printing Office, Washington, D.C. 20402, Sept. 1967, 20 cents).*
The NBS Center for Computer Sciences and Technology was established in 1965 to perform the Bureau's work in the field of computer technology—a broad program of standardization activities, applied research, and services to Federal agencies. Work on standards includes that on USASCII (for use in Federal procurement, under the terms of the Brooks Bill of October 1, 1965) and on optical character recognition. Services to other branches of government include providing data processing services, computational assistance, and consultation. The activities of the center's Technical Information Exchange and the continued experimentation with computers will have industry-wide benefits.

Key Words: Brooks Bill; computer standards; computer technology; data processing; government.

Midpoint quadrature formulas, S. Haber, *Math. Compt.* **21,** *No. 100, 719–721 (Oct. 1967).*
A family of quadrature formulas for the interval (0, 1) can be defined by partitioning the interval into subintervals and taking as nodes the midpoints of these intervals, with the lengths of the intervals serving as coefficients. The errors of these formulas are determined.

Key Words: Numerical analysis; quadrature; integration; computing.

The HAYSTAQ experiment, H. W. Hayward and S. J. Tauber, *Proc. ICIREPAT Fifth Annual Meeting, London, England, Aug. 31–*Sept. 10, 1965, Chapt. 26, pp. 337–*350 (Thompson Book Co., Washington, D.C., 1967).*
The background of the HAYSTAQ system is recapitulated. Shortcomings of an earlier chemical structure representation are reviewed; the scope and some advantages of the Hayward notation are stated. Suggestions are made for representing mixtures and classes of compounds. The scope is stated of notations for classes of reactions. The organization of files of chemical information and patterns of retrieval are discussed. Capabilities, limitations, and future implications of the techniques evolved are pointed out.

Key Words: Chemistry; compounds; computer; file organization; HAYSTAQ; Hayward; information retrieval; linear notation; Markush; mixtures; reactions; representations; screens; structures; topological codes.

Spectral irradiances as determined through the use of prism and filter spectroradiometric techniques, W. E. Schneider, R. Stair, and J. K. Jackson, *Appl. Opt.* **6,** *No. 9, 1479–1486 (Sept. 1967).*
Two spectroradiometers, one based on a conventional prism monochromator and the other on a system employing narrow band-pass interference filters, have been set-up and independently used in the determination of the spectral irrandiances of a number of sources over the wavelength range 0.25 μm to 2.5 μm. Basically, the method of calibration for each system consists of comparing the spectral irradiance of the source under investigation to that of an NBS standard of spectral irrandiance. The results obtained with each system on a number of "continuous" sources agree to about one percent whereas the differences in the spectral irradiances obtained with the two-set-ups on a number of line sources range up to several percent.

Key Words: Radiometry; spectral irradiance; prism-spectroradiometer; filter-spectroradiometer; measurement techniques; sources.

Anomalous heat capacity of TiNi, H. A. Berman, E. D. West, and A. G. Rozner, *J. Appl. Phys.* **38,** *No. 11, 4473–4476 (Oct. 1967).*
Calorimetric measurements on a sample of TiNi (50 atomic percent Ti) show that the heat-capacity maximum at approximately 87 °C represents a higher-order transition. The transition was shifted to lower temperatures each time the material was heated through the transition from slightly above room temperature to about 150–200 °C. The transition enthalpy decreased in three such cycles from 4150 to 3375 J/mole TiNi.

Key Words: Titanium-nickel heat capacity; titanium-nickel phase transition.

Correlation measurement in a turbulent flow using high-speed computing methods, F. N. Frenkiel and P. S. Klebanoff, *Phys. Fluids* **10,** *No. 8, 1737–1747 (Aug. 1967).*
Third-order time-correlations downstream of a grid were measured with a hot-wire anemometer using high-speed computing methods.

The nonlinear response of the hot-wire to the fluctuations of velocities is taken into account as well as the effect of transverse velocities. It is found that the third-order correlations are substantially different from previous results and demonstrate that the assumption of isotropy is not adequate for these correlations downstream of a grid. The nonlinear response does not significantly affect the difference $\overline{u_1^2 u_2} - \overline{u_1 u_2^2}$. Since previous conclusions concerning the nature of third-order correlations were based on the measurements of such differences they masked the effects of nonlinearity on the individual correlations. Correlations of fifth-order are also presented and their relations to the third-order correlation are discussed. Although the nonlinear corrections are quite important for odd-order correlations they are negligible for correlations of even-order.

Key Words: Turbulence; grid; hot-wire anemometer; nonlinear response; correlations; odd-order; even-order; isotropy.

Effect of a sinusoidal excitation amplitude on the performance of an atomic-beam spectrometer, J. H. Shirley, *Phys. Rev.* **160,** *No. 1, 95–99 (Aug. 5, 1967).*
A theoretical analysis has been made of the transition probabilities for a Rabi-type atomic beam spectrometer in which the exciting field amplitude seen by the atoms has a sinusoidal rather than a rectangular envelope. The time-dependent Schrödinger equation was integrated numerically and a velocity average of the transition probabilities performed. The results indicate that the line width increases as the fourth root of the excitation power and that frequency shifts due to coupling of the exciting field with other atomic states can be reduced by an order of magnitude.

Key Words: Atomic beam; transition probability; velocity average; frequency shift; Rabi spectrometer; Schrödinger equation.

Ellipsometric-potentiostatic studies of iron passivity, I. Anodic film growth in slightly basic solutions, J. Gruger and J. Calvert, *J. Electrochem. Soc.* **114,** *No. 12, 1265–1267 (Dec. 1967).*
Cathodically reduced iron was anodically oxidized to potentials in the passive region of the anodic polarization curve at passive potentials in nearly neutral sodium borate-boric acid solutions by means of a potentiostat. The kinetics of film growth were studied using an ellipsometer coupled with a high speed recording technique, which enabled a determination of the rate of film formation for times less than one second. This study of the kinetics of film growth using a non-electrochemical technique agreed with kinetic results based on total charge measurements.
Three states of growth were detected: (1) *First Stage*—growth limited by the diffusion of oxidizing species through solution. (2) *Second Stage*—start of limitation of growth of film. A combination of several processes difficult to characterize by any rate law. (3) *Third Stage*—growth obeying either a direct or indirect logarithmic rate law. The latter was found to imply that the passive film consisted of an outer layer poorly conductive for electrons.

Key Words: Ellipsometry; potentiostat; anodic oxidation; kinetics; iron oxide films; iron and passivity.

Laser harmonics useful for frequency translation, W. S. Lovell, M. M. Anderson, and F. E. Seiller, *Appl. Opt.* **6,** *No. 8, 1430–1432 (Aug. 1967).*
Accidental coincidences between laser fundamental and harmonic frequencies usable (in principle) for frequency translation are tabulated.

Key Words: Laser harmonics; frequency translation; accidental coincidences; frequency locking.

Some techniques used in the study of stress corrosion cracking, H. L. Logan, *Am. Soc. Testing Mater. Stress Corrosion Testing Spec. Tech. Publ. 425, 127–144 (1967).*
Techniques used at the National Bureau of Standards in the study of stress-corrosion cracking of metals are described together with precautions taken in these investigations. Especially designed specimen of low carbon and stainless steels and a titanium alloy and supplementary techniques for obtaining data as to the mechanism of the stress-corrosion process are also described. A specimen and technique recently used to determine whether hydrogen plays a part in the delayed failures of high strength steels in chloride solutions is described.

Key Words: Stress-corrosion; experimental techniques for stress corrosion testing; hydrogen embrittlement; low carbon steels; high strength steels; stainless steels; titanium alloys.

Strain-wave propagation in strips of natural rubber subjected to high-velocity transverse impact, J. C. Smith and C. A. Fenstermaker, *J. Appl. Phys.* **38,** *No. 11, 4218–4224 (Oct. 1967).*
If a flexible filament, marked at intervals along its length is struck transversely by a flying projectile, high speed photography reveals a shifting of the marks caused by passage of a strain wave, and analysis of these shifts provides data on the strain and average strain velocity in the wave. Tests were performed on strips of lightly vulcanized natural rubber at transverse impact velocities up to 65 m/s, and the resulting strain-velocity distributors analyzed for viscoelastic effects. The analysis showed that although creep effects were small in the observation time interval of 1 msec to 8 msec after impact, significant creep must have occurred at the point of impact within the first millisecond, and additional significant creep occurs at times greater than 8 msec. The strain wave front velocity calculated from the quasi-static stress-strain curve was 35.2 m/s, but a value of approximately 60 m/s was observed in the tests. The strain at the wave front, however, tended to attenuate as the wave propagated causing a progressive decrease in the observed value of the strain wave front velocity.

Key Words: Strain waves; natural rubber; viscoelasticity; impact testing; high-speed photography.

Superconducting transition temperatures of semiconducting $SrTiO_3$, C. S. Koonce, M. L. Cohen, J. F. Schooley, W. R. Hosler, and E. R. Pfeiffer, *Phys. Rev.* **163,** *No. 2, 380–390 (Nov. 10, 1967).*
The superconducting transition temperature T_c of $SrTiO_3$ has been measured for specimens having electron carrier concentrations n_c from 6.9×10^{18} cm^{-3} to 5.5×10^{20} cm^{-3}. The curve exhibits a maximum in T_c for n_c near 9×10^{19} cm^{-3}. The transition temperature has also been calculated using one adjustable parameter ξ, the intervalley deformation potential, in addition to the known normal-state properties of $SrTiO_3$. A good fit to the experimental curve is obtained.

Key Words: Semiconductors; $SrTiO_3$; superconductivity; transition temperatures.

The "memory effect" in silver iodide, G. Burley, *Act. Cryst.* **23,** *Part 1, 1–5 (July 1967).*
Radial distribution and least squares site occupation analyses were performed on powder diffraction patterns of the high temperature phase of silver iodide taken at 155 °C and 250 °C. A preferential occupation of certain sites by the silver atoms occurs near the transition temperature at 147 °C, involving those silver atom positions nearest to those in the low-temperature wurtzite- and sphalerite-type structures, respectively. The regeneration of a particular derivative low-temperature structure is thus facilitated, and a crystallographic explanation can be given for the observed "memory effect."

Key Words: Crystallography; structure memory; silver iodide; structure; alpha-phase; site-occupation.

Transmission through aluminum of beta-particles emitted by infinitely-thick sources, R. H. Rodriguez-Pasques, P. A. Mullen, G. A. George, and J. E. Harding, *Intern. J. Appl. Radiation Isotopes* **18,** *No. 12, 835–847 (1967).*
The problem of determining the energy of beta particles emitted from sources containing low concentrations of radioactive substances is examined. Transmission curves of beta particles emitted by "infinitely-thick" disc-shaped sources were obtained with two different detectors and compared to the curves similarly obtained for beta particles coming from very thin "weightless" deposits on similar solid discs. Different matrix materials and beta-particle energies were used. The curves were studied for shape, secondary radiations and half-thickness. A series of curves were also obtained from four different potassium-salt thick sources, in order to investigate possible influences from variations of effective atomic number. No substantial difference was found between the curves corresponding to the three types of sources, in connection with half-thickness-maximum-energy relationship.
Guiding rules are proposed for the determination of maximum beta-ray energies by means of absorption studies and half-thickness determination.

Key Words: Low-level; beta absorption; beta-particle energy; infinitely-thick sources; half thickness; synthetic beta sources; transmission curves; beta-particle transmission.

Other NBS Publications

J. Res. NBS 72A (Phys. and Chem), No. 2 (March-April 1968), $1.00.

Constant pressure flame calorimetry with fluorine II. The heat of formation of oxygen difluoride. R. C. King and G. T. Armstrong.

The heat of formation of boron carbide. E. S. Domalski and G. T. Armstrong.

Solubility of tris(hydroxymethyl)aminomethane in water-methanol solvent mixtures and medium effects in the dissociation of the protonated base. P. Schindler, R. A. Robinson, and R. G. Bates.

Calibration of the nickel dimethylglyoxime spectral shift at pressures to 20 kilobars for use in spectroscopic pressure measurement. H. W. Davis.

Second virial coefficient of He^4 in the temperature range from 2 to 20 °K. M. E. Boyd, S. Y. Larsen, and H. Plumb.

Diffusion rates in organic nuclear materials. A. L. Dragoo.

Effect of oxide additions on the polymorphism of tantalum pentoxide. (system Ta_2O_5-TiO_2). J. L. Waring and R. S. Roth.

Effect of statistical counting errors on wavelength criteria for x-ray spectra. J. S. Thomsen and F. Y. Yap.

Thermodynamic properties of ammonia as an ideal gas. L. Haar.

J. Res. NBS 72A (Phys. and Chem.), No. 3 (May–June 1968), $1.00.

Jump rates for point defects in special positions held by a trapping center of noncubic symmetry. H. S. Peiser and J. B. Wachtman, Jr.

The thermodynamics of the ternary system: water-potassium chloride-calcium chloride at 25 °C. R. A. Robinson and A. K. Covington.

Force field for SiF_4. I. W. Levin and S. Abramowitz.

Blemish formation in processed microfilm. C. I. Pope.

Absolute isotopic abundance ratios of common, equal-atom, and radiogenic lead isotopic standards. E. J. Catanzaro, T. J. Murphy, W. R. Shields, and E. L. Garner.

Role of nickel in Al–10 percent Si composites containing nickel-coated sapphire whiskers. H. Yakowitz, W. D. Jenkins, and H. Hahn.

J. Res. NBS 72A (Phys. and Chem.), No. 4 (July–August 1968), $1.00.

Mass spectrometric study of photoionization. X. Hydrogen chloride and methyl halides. M. Krauss, J. A. Walker, and V. H. Dibeler.

The fourth and fifth spectra of vanadium (V IV and V V). L. Iglesias.

Variation of absorptance-curve shape with changes in pigment concentration. G. L. Howett.

Periodic acid, a novel oxidant of polycyclic aromatic hydrocarbons. A. J. Fatiadi.

A galvanic cell with a low emf-temperature coefficient. G. N. Roberts and W. J. Hamer.

Synthesis of cerite. J. Ito.

Tables of collision integrals for the (m, 6) potential function for 10 values of m. M. Klein and F. Smith.

Spectrum of relaxation times in GeO_2 glass. A. Napolitano and P. B. Macedo.

Resumé of values of the Faraday. W. J. Hamer.

J. Res. NBS 72B (Math. Sci.), No. 2 (April–June 1968), 75 cents.

The probability of an equilibrium point. K. Goldberg, A. J. Goldman, and M. Newman.

Differentiable generalized inverses. J. Z. Hearon and J. W. Evans.

On spaces and maps of generalized inverses. J. Z. Hearon and J. W. Evans.

Principal submatrices V: Some results concerning principal submatrices of arbitrary matrices. R. C. Thompson.

Mathematical basis for the plasma kinetic equations (BBGKY). J. J. Sopka.

On the diffusion of an ion sheet in Poiseuille flow. S. Jarvis, Jr.

A class of thickness-minimal graphs. A. M. Hobbs and J. W. Grossman.

Compendium of *ab initio* calculations of molecular energies and properties, M. Krauss, Tech. Note 438 (Dec. 1967), 70 cents.

Operations research. Proceedings of a conference for Washington area government agencies, April 20, 1966, Ed. J. A. Joseph, Misc. Publ. 294 (Dec. 1967), 25 cents.

The hyperbolic character of certain experimental results which tend toward limiting values, A. F. Kirstein, Tech. Note 435 (Nov. 1967), 15 cents.

A theorem on arbitrary functions, S. Haber, Am. Math. Monthly **74,** No. 8, 973–975 (Oct. 1967).

Algorithms for utilizing Hayward chemical structure notations, S. J. Tauber, G. R. Bolotsky, G. F. Fraction, C. L. Kirby, and G. R. Reed, Proc. ICIREPAT Fifth Annual Meeting, London, England, Aug. 31–Sept. 10, 1965, Chapt. 27, pp. 351–377 (Thompson Book Co., Washington, D.C., 1967).

Analysis of rotationally misaligned stators in the rotary-vane attenuator, W. Larson, IEEE Trans. Instr. Meas. **IM–16,** No. 3, 225–231 (Sept. 1967).

Born-model calculation of point-defect formation energies in alkaline-earth fluorides, A. D. Franklin (Proc. 2nd Meeting Point Defects in Non-metallic Solids, University of Sussex, Brighton, England, Sept. 26–28, 1966), Proc. British Ceramic Soc. **9,** 15–24 (July 1967).

Dissociation of N_2^+ and O_2^+ by electron impact, B. Van Zyl and G. H. Dunn, Phys. Rev. **163,** No. 1, 43–45 (Nov. 5, 1967).

Effect of chain twisting on the effective barrier to reorientation for a hindered rotator, G. Williams, J. I. Lauritzen, Jr., and J. D. Hoffman, J. Appl. Phys. **38,** No. 11, 4203–4208 (Oct. 1967).

Electron affinity of helium via laser photodetachment of its negative ion, B. Brehm, M. A. Gusinow, and J. L. Hall, Phys. Rev. Letters **19,** No. 13, 737–741 (Sept. 5, 1967).

Entropy and susceptibility of a pure dipole-dipole substance, J. R. Peverley and P. H. E. Meijer, Phys. Stat. Sol. **23,** No. 1, 353–360 (1967).

40 years of precise measurement, W. G. Brombacher, Instr. Control Systems **40,** No. 9, 87–92 (Sept. 1967).

Gas-phase photolysis of ethyl iodide at 2537 and 2288 Å. Reactions of hot ethyl radicals with added hydrocarbons, R. E. Rebbert and P. Ausloos, J. Chem. Phys. **47,** No. 8, 2849–2855 (Oct. 15, 1967).

Inelastic scattering of cold neutrons in polycrystalline gray tin, V. W. Myers, J. Phys. Chem. Solids **28,** 2207–2210 (1967).

Inelastic scattering of kilovolt electrons by solids and liquids: determination of energy losses, cross sections, and correlations with optical data, C. J. Powell, Health Phys. **13,** No. 12, 1265 (1967).

Mass-spectrometric study of photoionization. VI. O_2, CO_2, COS, and CS_2, V. H. Dibeler and J. A. Walker, J. Opt. Soc. Am. **57,** No. 8, 1007–1012 (Aug. 1967).

Matrix-isolation study of the reaction of carbon atoms with HCl. The infrared spectrum of the free radical HCCl, M. E. Jacox and D. E. Milligan, J. Chem. Phys. **47,** No. 5, 1626–1633 (Sept. 1, 1967).

Neutron-scattering study of hindered rotations in methylbenzenes, J. J. Rush, J. Chem. Phys. **47,** No. 10, 3936–3941 (Nov. 15, 1967).

Neutron-scattering study of low-frequency modes in urea and ferroelectric thiourea, J. J. Rush, J. Chem. Phys. **47,** No. 10, 4278–4279 (Nov. 15, 1967).

NMR studies of inorganic fluorides. III. Si_3F_8, R. B. Johannesen, J. Chem. Phys. **47,** No. 3, 955–960 (Aug. 1, 1967).

NMR studies of inorganic fluorides. IV. Relative signs of coupling constants in CH_3SiF_3, $HSiF_3$, and HPF_2, R. B. Johannesen, J. Chem. Phys. **47,** No. 8, 3088–3089 (Oct. 15, 1967).

N_2O bond dissociation energy by photon impact, V. H. Dibeler, J. Chem. Phys. **47,** No. 6, 2191–2192 (Sept. 15, 1967).

Observing the effect of a change in mass on deBroglie wavelength: the 600-Å bands of $^3He_2$, A. L. Smith, J. Chem. Phys. **47,** No. 4, 1561–1562 (Aug. 15, 1967).

Pair production by photons on electrons, K. J. Mork, Phys. Rev. **160,** No. 5, 1065–1071 (Aug. 1967).

Phenylhydrazono-phenylazo tautomerism. Part II. Structures of 2-oxo-1, 3-bis(phenylhydrazono) compounds and related compounds, A. J. Fatiadi and H. S. Isbell, Carbohydr. Res. **5,** 302–319 (1967).

Photolysis of ethylene at 1048–1067 A. Reactions of C_2H_4+ and fragmentation of the superexcited ethylene molecule, R. Gorden, Jr. and P. Ausloos, J. Chem. Phys. **47,** No. 5, 1799–1806 (Sept. 1, 1967).

Probability distribution of the radius of gyration of a flexible polymer, S. R. Coriell and J. L. Jackson, J. Math. Phys. **8,** No. 6, 1276–1284 (June 1967).

Rotational excitation of diatomic molecules by slow electrons; application to H_2, N. F. Lane and S. Geltman, Phys. Rev. **160,** No. 1, 53–67 (Aug. 1967).

Stretch scheme, a shell-model description of deformed nuclei, M. Danos and V. Gillet, Phys. Rev. **161,** No. 4, 1034–1044 (Sept. 20, 1967).

Structure, isomerization, and cleavage of 1,2-bis(dichloroboryl)-ethylene, T. D. Coyle and J. J. Ritter, J. Am. Chem. Soc. **89,** 5739–5740 (1967).

Superposition of configurations and atomic oscillator strengths-carbon I and II, A. W. Weiss, Phys. Rev. **162,** No. 1, 71–80 (Oct. 5, 1967).

SU(3), meson-baryon scattering, and asymptotic limits, S. Meshkov and G. B. Yodh, Phys. Rev. Letters **19,** No. 10, 603–608 (Sept. 4, 1967).

Twin configurations in FCC dendrites, J. W. Faust, Jr., F. Ogburn, D. Kahan, and A. W. Ruff, Jr., J. Electrochem. Soc.: Solid State Science **114,** No. 12, 1211–1212 (Dec. 1967).

User reaction as a system design tool at CFSTI, P. F. Urbach, Proc. Fourth Annual National Colloquium on Information Retrieval, May 3–4, 1967, Ed. A. B. Tonik, pp. 7–18 (International Information, Inc., Philadelphia, Pa., 1967).

**Publications for which a price is indicated are available by purchase from the Superintendent of Documents, U.S. Government Printing Office, Washington, D.C. 20402 (foreign postage, one-fourth additional). The NBS non-periodical series are also available from the Clearinghouse for Federal Scientific and Technical Information, Springfield, Va. 22151. Reprints from outside journals and the NBS Journal of Research may often be obtained directly from the authors.*

U.S. GOVERNMENT PRINTING OFFICE : 1968 OL—306-528

UNIVERSITY MICROFILMS INC
SERIALS SECTION
300 NORTH ZEEB ROAD
ANN ARBOR MICHIGAN 48106

UNI
GOVERNMENT PRINTING OFFICE
DIVISION OF PUBLIC DOCUMENTS
WASHINGTON, D.C. 20402

OFFICIAL BUSINESS

POSTAGE AND FEES PAID
U.S. GOVERNMENT PRINTING OFFICE

JOURNAL OF RESEARCH of the National Bureau of Standards — Vol. 72C, No. 3 — July–September 1968
C. Engineering and Instrumentation

Contents

	Page
Gas density balance design considerations. E. C. Creitz.	187
Standard mismatch—the production of controlled small reflections in waveguides. L. Lewin.	197
Viscoelastic behavior of dental amalgam. P. L. Oglesby, G. Dickson, M. L. Rodriguez, R. M. Davenport, and W. T. Sweeney.	203
The steady-state creep behavior of dental amalgam. George Dickson, Philip Oglesby, and Ruth Davenport.	215
Publications of the National Bureau of Standards.	219

Library of Congress Catalog Card Number: 62–3900

For sale by the Superintendent of Documents, U.S. Government Printing Office, Washington, D.C. 20402. Price 75¢ (single copy). Subscription price: $2.75 a year; 75¢ additional for foreign mailing.
UNITED STATES GOVERNMENT PRINTING OFFICE, WASHINGTON : 1968